NASA Technical Memorandum 108533

Microgravity Processing and Photonic Applications of Organic and Polymeric Materials

(MSFC Center Director's Discretionary Fund Final Report, Project No. 95–26)

D.O. Frazier, B.G. Penn, D.D. Smith, and W.K. Witherow
Marshall Space Flight Center • MSFC, Alabama

M.S. Paley and H.A. Abdeldayem
Universities Space Research Association • Huntsville, Alabama

National Aeronautics and Space Administration
Marshall Space Flight Center • MSFC, Alabama 35812

March 1997

ACKNOWLEDGMENTS

The authors are grateful for support from NASA's Office of Life and Microgravity Science and Marshall Space Flight Center's Center Director's Discretionary Fund. We are also grateful to Hari Sunkara for helpful suggestions after reviewing the manuscript.

TABLE OF CONTENTS

I. INTRODUCTION 1

A. Third-Order Materials for Optical Switching 1
B. Second-Order Materials for Electro-Optic Applications 2
C. Material Limitations 4
1. Dispersion and Loss 4
2. Two-Photon Absorption 4
D. Candidate Materials 7
1. Fused Silica Fibers Versus Conjugated Organics 7
2. Gravitational Effects in Processing Organic and Polymeric Films 8

II. GROWTH OF THIN FILMS BY VAPOR DEPOSITION 11

A. Phthalocyanine Thin Films 11
B. Polydiacetylene Thin Films 19
1. Second- and Third-Order NLO Properties of PDA's 19
2. Potential Benefits of Microgravity Processing 20

III. GROWTH OF THIN FILMS BY SOLUTION PROCESSES 29

A. Ultraviolet Solution Polymerization 29
1. Polydiacetylene Films 29
2. Third-Order NLO Properties of Films 30
3. Fluid Dynamic Analysis 31
4. Transport of Particles from Bulk Solution 32
5. Effects of Convection on Kinetics, Morphology, and Microstructure 35
6. Growth of Films in Microgravity 36
B. Polymer Thin Films by Electrochemical Polymerization 36

IV. PROTOTYPE DEVICES BASED ON SECOND- AND THIRD-ORDER NLO ORGANICS AND POLYMERS 39

A. Electro-Optic Polymer Advances 39
B. All-Optical Switching 40

REFERENCES 43

LIST OF ILLUSTRATIONS

1. Effect of TPA on an NLDC. The coupler is initially in a crossed state. Increasing input power perturbs coupling which causes switching, suppressed by the presence of TPA 5

2. Elimination of induced absorption in HITCI by the addition of small Au particles. For each *z*-scan the peak power was P_i = 0.16 MW and the on-axis peak irradiance at focus was I_o = 2.1 GW/cm^2 7

3. PDAMNA circuit photodeposited onto UV transparent substrates using the radiation from an argon ion laser: (a) demonstration pattern on a quartz disk, and (b) enlarged image of an actual Mach-Zehnder interferometer on a glass microscope slide 9

4. Metal-free Pc (H_2Pc) 11

5. Trinitro-substituted boron subPc 12

6. CuPc films epitaxially vapor-deposited onto copper substrate: (a) μ-g deposition of CuPc epilayer, and (b) 1-g deposition of CuPc epilayer (courtesy of 3M Corporation) 15

7. (a) Time-dependent transmittance through a metal-free Pc film (230-nm thick), using a cw He-Ne laser at 632.8 nm and 30 mW power. The dotted curve represents the experimental data, while the solid line represents a single exponential theoretical fit; (b) The dotted line represents laser stability throughout the experiment, while the solid line is the corresponding straight-line fit 16

8. The bistability loop of an 833-nm metal-free Pc film using a chopped cw He-Ne laser at 632.8 nm: (a) the input pulse, (b) the transmitted pulse, and (c) hysteresis switching constructed from (b) 17

9. The bistability loops for different timespans of a metal-free Pc film of 232.5-nm thickness using a cw He-Ne laser. Timespans between successive points are (a) 3.84 sec, (b) 10 sec, (c) 342 sec, and (d) 1,800 sec. (a) shows the number sec, least prominent bistability loop while (b), (c), and (d) show a minimal effect of the timespan between points 18

LIST OF ILLUSTRATIONS (continued)

10. Experimental and theoretical fitting of saturable absorption of a metal-free Pc film (232.5-nm thickness) at 632.8 nm from a cw He-Ne laser. The corresponding saturation intensity is 19.8×10^3 W/cm^2 19

11. Structure of PDA repeat unit 20

12. Diacetylene monomer, DAMNA 21

13. Vapor deposition cell for PVT of DAMNA 22

14. Axisymmetric flow in the $\theta = 0°–180°$ plane in cell in which deposition occurs with cell oriented vertically 23

15. Flow in the $\theta = 0°–180°$ plane in cell in which deposition occurs with cell tilted 45° to vertical axis 24

16. Flow in the $\theta = 90°–270°$ plane in cell in which deposition occurs with cell tilted 45° to vertical axis 25

17. Absorbance as function of wavelength for vapor-deposited film after 30 minutes of deposition for (a) a vertically oriented cell, and (b) a tilted cell 27

18. (a) PDA thin film growth chamber, and (b) masked PDAMNA film on glass 30

19. PDAMNA films grown in two different orientations: (a) films grown with the chamber horizontal, and (b) films grown with the chamber vertical 34

20. PDAMNA films grown in space. The best space-grown films clearly exhibit fewer particles than the best ground-based films 37

21. (a) Mach-Zehnder interferometer, (b) NLO loop mirror, and (c) nonlinear directional coupler and their electronic analogs 40

LIST OF TABLES

1. Component proportions of HITCI/Au composite 6

2. $\chi^{(3)}$ of vapor-deposited thin films of Pc's measured at a wavelength of 1.9 μm[58] 13

3. Representative absorbance intensities from scanning an approximately 1-cm-diameter spot in similar vicinities of DAMNA films formed during vapor deposition 28

TECHNICAL MEMORANDUM

MICROGRAVITY PROCESSING AND PHOTONIC APPLICATIONS OF ORGANIC AND POLYMERIC MATERIALS
(MSFC Center Director's Discretionary Fund Final Report, Project No. 95–26)

I. INTRODUCTION

In recent years, a great deal of interest has been directed toward the use of organic materials in the development of high-efficiency optoelectronic and photonic devices. There is a myriad of possibilities among organics which allow flexibility in the design of unique structures with a variety of functional groups. The use of nonlinear optical (NLO) organic materials as thin film waveguides allows full exploitation of their desirable qualities by permitting long interaction lengths and large susceptibilities allowing modest power input.[1] There are several methods in use to prepare thin films such as Langmuir-Blodgett (LB) and self-assembly techniques,[2–4] vapor deposition,[5–7] growth from sheared solution or melt,[8 9] and melt growth between glass plates.[10] Organics have many features that make them desirable for use in optical devices such as high second- and third-order nonlinearities, flexibility of molecular design, and damage resistance to optical radiation. However, their use in devices has been hindered by processing difficulties for crystals and thin films.

In this chapter, we discuss photonic and optoelectronic applications of a few organic materials and the potential role of microgravity on processing these materials. It is of interest to note how materials with second- and third-order NLO behavior may be improved in a diffusion-limited environment and ways in which convection may be detrimental to these materials. We focus our discussion on third-order materials for all-optical switching, and second-order materials for frequency conversion and electro-optics.

A. Third-Order Materials for Optical Switching

Optical fiber communication systems have undergone stunning growth over the past decade. The technologies that have arisen in support of these systems have been incredibly fortuitous. The operating wavelength of erbium-doped amplifiers, for instance, serendipitously coincides with the minimum loss wavelength of fused silica fibers. But, even as fiber optic networks have been implemented on a universal scale, electronic switching is still the main routing method. Although fibers have dramatically increased node-to-node network speeds, electronic switching will limit network speeds to about

50 Gb/sec. Already, it is apparent that terabit-rate speeds will soon be needed to accommodate the 10–15 percent/month growth rate of the Internet and the increasing demand for bandwidth-intensive data such as digital video.[11]

All-optical switching using NLO materials can relieve the escalating problem of bandwidth limitations imposed by electronics. Several important limitations need to be overcome such as the need for high $\chi^{(3)}$ materials with fast response and minimum absorption (both linear and nonlinear), development of compact laser sources, and reduction of the switching energy. The goal of minimizing optical loss obviously depends on processing methods. For solution-based processes, such as solution crystal growth, electrodeposition, and solution photopolymerization, it is well known that thermal and solutal density gradients can initiate buoyancy-driven convection. Resultant fluid flows can affect transport of material to and from growth interfaces and become manifest in the morphology and homogeneity of the growing film or crystal. Likewise, buoyancy-driven convection can hinder production of defect-free, high-quality crystals or films during crystal and film growth by vapor deposition.

The guided-wave materials used most commonly have been inorganic fibers and semiconductors. Less developed but highly promising are organic materials such as conjugated polymers, which possess large nonlinearity with fast response times, are more easily tailored at a molecular level, and more malleable than their inorganic counterparts. One of the major challenges for proponents of organic materials is to find cheap, reliable methods of waveguide fabrication that take advantage of existing technologies. Processing techniques and choices of materials should result in a minimization of both scattering and absorption losses. One of the main reasons that organic and polymeric materials are not more strongly competitive with silica fibers for switching applications is due to the maturity of silica fiber processing.

B. Second-Order Materials for Electro-Optic Applications

Applications of materials with second-order nonlinearity include frequency conversion, high-density data storage, and electro-optic modulators and switches. The first demonstration of second harmonic generation was in quartz,[12] and it has traditionally been observed in inorganic crystals. A decade later it was demonstrated that the second-order nonlinearity may be several orders of magnitude larger in organic crystals possessing delocalized π-electron systems in which intramolecular charge transfer occurs between electron donor and acceptor substituents.[13] While organic materials may offer larger nonlinearities than inorganic crystals, the utilization of organic crystals is limited by the small number of molecules with large hyperpolarizabilities that have a noncentrosymmetric crystalline state (11 of the 32 crystal classes possess inversion symmetry and cannot be used as $\chi^{(2)}$ materials). Moreover, the maturity of inorganic crystal growth is relatively advanced while that of organic crystal growth has not had the necessary time for comparable development.

Whereas the second-order nonlinearity in inorganic systems is a bulk effect ascribable to crystalline structure, the primary contribution to bulk nonlinearity for organic systems is due to the ensemble of nonlinearly responding molecules. Van der Waals forces between mers (molecular units)

are small and the induced dipoles result most directly from the external field. This provides an added degree of flexibility for organic materials since the required asymmetry does not require crystalline structure but instead may be achieved in amorphous geometries. For example, instead of relying on the art of crystal growth, electric field poling of polymers containing the nonlinear chromophore may be used to induce macroscopic asymmetry. Alternatively, self-assembly or liquid crystal ordering can achieve the required asymmetry, possibly encouraged in the environmental quiescence offered by reduced convection during microgravity processing.

In order to take advantage of the large nonlinearities in organic materials resulting from π-electron mobility while also utilizing the mechanical and thermal properties of inorganic crystals, some researchers have turned to a semiorganic approach in which organic molecules are bound to an inorganic host by complexation or salt formation. For example, semiorganic single crystals of L-histidine tetrafluoroborate (HFB) have demonstrated five times the effective second-order nonlinearity of potassium dihydrogen phosphate (KDP).[14] Single crystals are easily obtained from solution and crystals are thermally stable with a decomposition temperature of 205 °C. Solution crystal growth has been performed repeatedly in microgravity, particularly for the study of protein crystal growth. Many organics, also good NLO materials, are amenable to solution growth and are ideal candidates for studies of the kinetics and fluid dynamics of solution growth processes. Knowledge of such processes can lead to significant improvement in crystals grown in space or on Earth. Several research tasks are underway to study the growth of bulk single crystals of important materials such as HFB, L-arginine phosphate, and several other organic and semiorganic molecules. There is certainly evidence that gravity could play a role in the growth of macromolecular crystals; e.g., protein crystals, as well as on solution polymerization processes. Rosenberger studied the temperature dependence of protein solubility, and applications to crystallization and growth kinetics. Within these studies he observed relative interfacial kinetics and bulk transport as functions of supersaturation and the resultant effects on the growth morphology of lysozyme and horse serum albumin.[15] Supersaturations driven by thermal fluctuations on the order of 1–2 °C during growth lead to significant optical and structural nonuniformity in a growing crystal. Pusey et al., using tetragonal lysozyme, showed that forced fluid flow rates of 30–40 mm/sec slow and eventually stop the growth of 10 μm crystals.[16 17] Cessation of growth occurred at flow rates as low as 2.5 mm/sec in some crystals, but growth persisted over a longer period of time than at higher fluid flow rates. The conclusion is that, for some crystals at least, even small convective flows are deleterious for growth of the crystal. The precise mechanism for this is not yet understood, but clearly the case is quite strong for studying the growth of certain organic and semiorganic crystals in microgravity environments.

It is, therefore, reasonable to consider that microgravity can play an important role in the formation of organic and semiorganic crystals for second-order applications. In the diffusion-limited regime of space, larger and more defect-free crystals may be grown, hence improving optical transparency and conversion efficiency. By different processing techniques, improved optical quality and molecular alignment have been observed in polydiacetylene (PDA) and phthalocyanine (Pc) thin films processed in microgravity or reduced convection environments. Perhaps of more immediate relevance, knowledge gained from low-gravity (low-g) experiments may enable the optimization of growth conditions on Earth.

C. Material Limitations

1. Dispersion and Loss

One limitation governing the propagation of pulses in a waveguide is the reshaping of the pulse due to group velocity dispersion (GVD). Each frequency component in the pulse sees a different refractive index and thus travels at a different speed through the medium, leading to a spreading or reshaping of the pulse. GVD is more important for short pulses since they contain more frequency components. This pulse spreading reduces the amount of information that can be carried and destroys the cascadability (the ability of the output of a device to reenter an identical device and behave similarly) of the system. However, a pulse also consists of different intensities. Each intensity can also see a different refractive index, due to the nonlinearity of the medium, and so travels at a different speed. The ability of a pulse to become reshaped due to the nonlinearity of the medium is known as self-phase modulation (SPM). For certain pulse shapes, GVD is exactly balanced by SPM and the pulse retains its shape over an infinite propagation distance in the absence of loss. These pulse shapes are known as solitons. In practice, however, solitons cannot propagate infinitely. The effect of dissipation decreases the peak power in the pulse, hence decreasing SPM. The result is that the soliton widens as it propagates. Two main sources of loss are operative in silica fibers—an intrinsic loss due to Rayleigh scattering and, superimposed on this, absorption due to hydroxide ion impurities in the melt.[18] Due to the maturity of silica fiber fabrication technology, impurities in the melt can be kept quite low. Microgravity processing may enable polymeric materials to become more competitive with silica fibers through the reduction of similar types of scattering loss mechanisms.

2. Two-Photon Absorption

A major setback in the development of an all-optical switch is the existence of nonlinear loss manifested by multiphoton absorption. The current strategy is to search for a truly nonresonant operating wavelength. To demonstrate the deleterious effects of multiphoton absorption, consider its effect on a simple device. A nonlinear directional coupler (NLDC) is a device in which two waveguides or fibers are brought close together such that their overlapping evanescent attenuations periodically transfer power back and forth between the guides as light propagates through the device.[19] The periodicity of phase-matched power transfer depends on channel separation and refractive index. Full power transfer occurs after one coupling length, L_c. When the length of the overlapping region equals the coupling length, all the power will be transferred to the neighboring guide. If the guide material has a large cubic nonlinearity (and hence, nonlinear refractive index, n_2), the coupling will be perturbed at high intensities due to an intensity-dependent phase mismatch in the guides, and at the switching power, the majority of the transmission will switch from one guide to the other. The majority of the coupler's output may then be toggled between the guides simply by raising and lowering the intensity.

Multiphoton absorption occurs when the intensity of the radiation causes virtual levels to become accessible. In centrosymmetric media, transition rules prohibit transitions between same parity states unless virtual levels are involved. Because two-photon absorption (TPA) is intensity-dependent, it varies with propagation distance. The result is that power transfer is accompanied by increasing TPA in the low

intensity guide and decreasing TPA in the high intensity guide such that complete switching does not occur or is suppressed (fig. 1). Mizrahi et al.[20] have shown that TPA places a fundamental constraint on the usefulness of any high $\chi^{(3)}$ material. Semiconductors, for example, are constrained to energies below half the band gap to avoid TPA.[21 22]

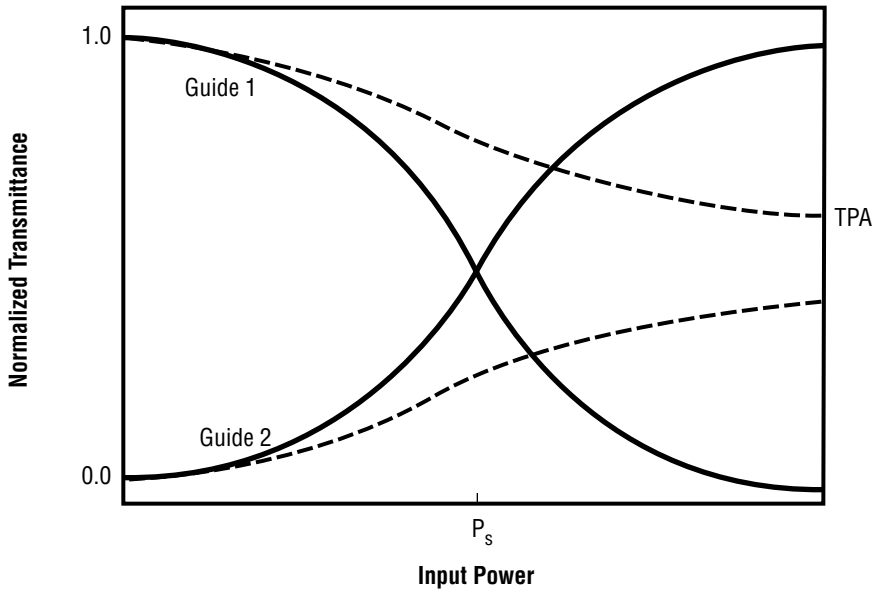

FIGURE 1.— Effect of TPA on an NLDC. The coupler is initially in a crossed state. Increasing the input power perturbs the coupling, resulting in switching, but the presence of the TPA suppresses switching.

An alternative approach based on materials architecture is also possible for eliminating induced absorption. Specifically, the nonlinear absorption in a material may be canceled by the addition of small metal particles. This approach is possible because of a counterintuitive consequence of local field effects that was first recognized by Hache et al.[23] They found that for gold nanoparticles in glass, the colloid as a whole demonstrated saturable absorption. However, the metal itself behaved quite differently, demonstrating induced absorption. Embedding the particles in a glassy matrix altered the sign of the nonlinear absorption as a result of the local field correction. The implication of Hache's finding is that there is a concentration somewhere between pure gold and the colloidal gold glass at which the imaginary part of the cubic susceptibility goes to zero. In fact, if the sign of $Im\chi^{(3)}$ is the same for each component, then by necessity there will actually be two concentrations at which $Im\chi^{(3)} = 0$. The smaller concentration crossing point is obviously more useful since it entails a lower amount of linear absorption and poses less of a challenge to fabricate. The significance and specificity of particle concentration demands careful control of metal particle dispersion. This requirement is also prevalent in crystal growth of certain semiconducting alloys where the optimum band gap is determined by alloy stoichiometry. Lehoczky et al. directionally solidified $Hg_{0.84}Zn_{0.16}Te$ alloy in microgravity with some success at purely diffusion-controlled growth to achieve the desired stoichiometry throughout

the space-grown crystal. However, unexpected transverse residual accelerations from the space shuttle environment resulted in some radial compositional variations.[24] The result stresses the difficulty in achieving precise concentrations during materials processing where thermal or concentration gradients arise, and could be fatally disruptive in terms of achieving a defined concentration objective. Considering difficulties in achieving diffusion-controlled growth, and other desirable gravitationally sensitive results during microgravity processing, ground-based attempts at overcoming these effects may prove futile. Where homogeneous dispersion and concentration are requisite in materials of interest, processing on Earth-orbiting platforms could offer distinct advantages.

To demonstrate the cancellation of photoinduced absorption in a composite system, Smith[25] performed open aperture *z*-scan measurements on a gold colloid prepared by the recipe of Turkevich[26] at various particle concentrations. A frequency-doubled Nd:YAG laser at 532 nm provided 30-ps, mode-locked pulses at a repetition rate of 10 Hz. Each concentration was placed in a 1-cm optical pathlength quartz cuvette on a track near the focus of the beam. The focal length of the lens was 33 cm and the full width half maximum (FWHM) beam diameter was 2.5 mm. The beam waist was measured to be $w_0 = 70\ \mu$m, corresponding to a Rayleigh diffraction length of $z_0 = 2.9$ cm.

Instead of TPA, however, the nonlinear mechanism was reverse saturable absorption. The system consisted of a known reverse saturable absorber $1,1',3,3,3',3'$-hexamethylindotricarbocyanine iodine (HITCI) in methanol and water. The proportions of dye, methanol, and water were held fixed. Since these chemicals form a solution, they may be considered as a single component, although their chemical association should be accounted for by a modification of the local field factor as described by Fröhlich.[27] The other component was the gold. The proportions of the various components are illustrated in table 1. Note that the same amount of dye, methanol, and water is used in each case and that the only variable is the concentration of gold. The *z*-scans for various concentrations of gold are displayed in figure 2. It can clearly be seen that the nonlinear absorption changes sign near curve 6. The experiment was repeated several times and the sign reversal was obvious each time. Note that curves 1–5 display a valley indicative of reverse saturable absorption. At the focus, however, a small secondary peak is observed. This peak corresponds to a saturation of the nonlinear absorption and was first reported by Swatton et al.[28] A four-level semiclassical model was used to describe the absorption of the dye.

TABLE 1.—*Component proportions of HITCI/Au composite.*

Curve Number	Gold Colloid (ml)	Water (ml)	123 μM Solution of HITCI (ml)	Methanol (ml)
1	0.0	2.75	0.4	0.6
2	0.5	2.25	0.4	0.6
3	1.0	1.75	0.4	0.6
4	1.5	1.25	0.4	0.6
5	1.9	0.85	0.4	0.6
6	2.0	0.75	0.4	0.6
7	2.2	0.55	0.4	0.6
8	2.5	0.25	0.4	0.6
9	2.75	0.00	0.4	0.6

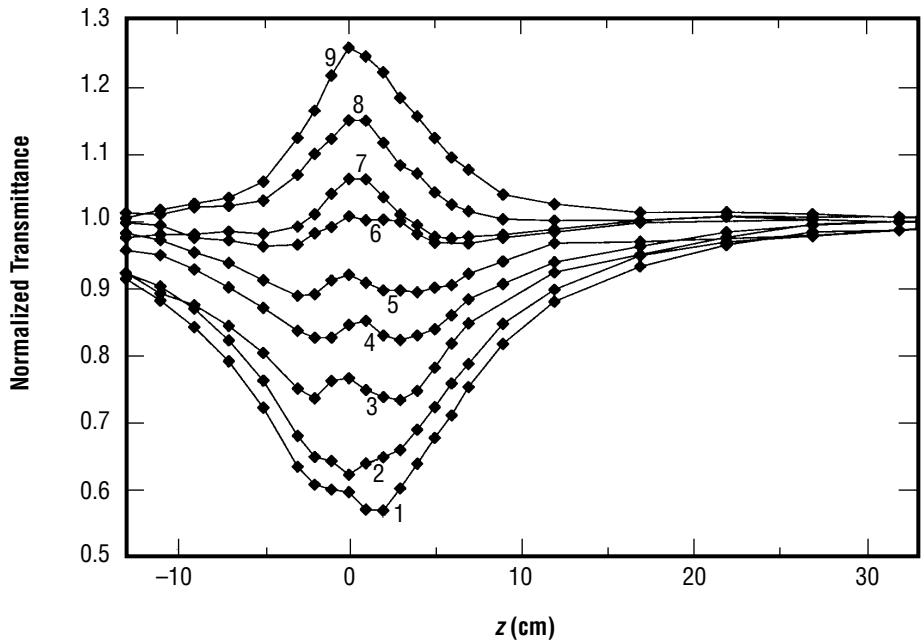

FIGURE 2.—Elimination of induced absorption in HITCI by the addition of small Au particles. For each *z*-scan the peak power was P_i = 0.16 MW and the on-axis peak irradiance at focus was I_o = 2.1 GW/cm^2.

D. Candidate Materials

1. Fused Silica Fibers Versus Conjugated Organics

Figures of merit have been proposed to describe the linear and nonlinear losses and the dispersion in candidate materials.[20 22 25 29–32] Fused silica fibers are attractive for optical communications systems because, although they have a relatively weak nonlinearity, they have among the highest figures of merit due to their low loss in the region 1.3–1.6 μm, known as the telecommunications window. Also, silica fibers exhibit anomalous (negative) dispersion for wavelengths greater than 1.3 μm, allowing solitons to propagate. The two wavelengths most commonly used for communications are the zero-dispersion wavelength of 1.3 μm and the low-loss wavelength of 1.55 μm. The wavelength of choice has become 1.55 μm, due to the availability of multiple-clad, dispersion-shifted fibers.

A rule of thumb for all-optical switches is that $\chi^{(3)} LI$ is constant,[11] where L is optical pathlength and I is intensity input. So, although silica fibers have a much lower cubic nonlinearity, $\chi^{(3)}$, the switching power can be much lower than that of other materials because there is almost no length limitation on a fiber; whereas, typically for a highly nonlinear material, the loss is much greater, imposing a length limitation. But simply increasing the switch's operating length does not take into account the dispersion or spreading of the pulse which becomes more important for very short pulses. For fused silica fibers the dispersion can be tuned negative to support solitons, but most highly

nonlinear materials have positive GVD in the telecommunications window and so cannot support solitons for these wavelengths. One way to decrease the switching energy but not the switching power is to use shorter pulses, however this also increases dispersion. Thus, for long pulses, fibers are not constrained by pulse spreading and can operate at lower powers but for short pulses, materials with higher nonlinearities may switch at lower powers due to GVD considerations. Asobe et al. have shown that for very short pulses, when GVD is taken into account, highly nonlinear conjugated polymers will operate at a lower switching energy than positive dispersion silica fibers.[32] As we will show, microgravity may be exploited to reduce the length limitation in polymeric waveguides.

Another reason for choosing highly nonlinear conjugated polymers over silica fibers is because of limitations which arise from the propagation design of the device. Switching in silica fibers requires very long lengths of fiber which can seriously reduce the switching time and result in cumbersome setups.

2. Gravitational Effects in Processing Organic and Polymeric Films

Two promising classes of organic compounds for optical thin films and waveguides are PDA's, which are conjugated zig-zag polymers, and Pc's, which are large ring-structured porphyrins. Epitaxial growth on ordered organic and inorganic substrates under various processing conditions have been useful for preparing highly oriented PDA and Pc films.[33–35] The degree of significance relating processing conditions to uniformity in thickness, degree of orientation, and optical properties for a specific processing technique is the general focus of work in this area.

A study on the effect of processing conditions relevant to thin-film deposition by various techniques is particularly difficult because of the possibility that convection may play a major role. It is a goal of some researchers to produce good quality anisotropic films, therefore, an important, yet understudied, requirement should be to assess the role of gravity during processing. This may be particularly true for the vapor deposition of diacetylenes where subsequent polymerization in the crystal is topochemical and occurs readily only when neighboring monomer molecules are sufficiently close and suitably oriented.[29]

Likewise, this requirement is equally viable for the vapor deposition of Pc's in view of the results of microgravity experiments by 3M Corporation involving the preparation of thin films of copper Pc (CuPc).[34−44] Indeed, a variety of microstructural forms was obtained in thin films of CuPc, dependent on processing methods and conditions. Small changes in processing parameters caused large changes in molecular orientation within the film. Microgravity-grown CuPc had several desirable features which indicate that the growth of organic films in low-g may result in better quality films for optical and electrical applications.[43 44] The dramatic 3M result was very encouraging and has been one source of optimism toward considering the microgravity environment of value for processing high-quality organic films. One goal of microgravity research on vapor-deposited organic films is to understand factors for improving film quality and optical properties. Important aspects of any study involving fluids, as in vapor transport, are driving mechanisms for heat transfer with natural convection and diffusion processes which determine flow profiles and temperature distributions.

A novel technique, recently discovered, for growing PDA thin films involves exposing a transparent substrate, in contact with diacetylene monomer solution, to ultraviolet (UV) light.[45] A polymer film deposits on the side of the substrate in contact with monomer in solution, and there are distinct gravitational effects which influence film quality. Good quality thin films elude growth from solutions absent of uniform flow fields and homogeneous temperature distributions near the substrate surfaces. The flow fields and temperature distributions during the polymerization process by exposure to UV light details the nature of gravitational influences on this process.

From a device perspective, the UV technique makes construction of extremely complex waveguides possible. Utilizing a computer-controlled *x-y* translation stage, programmed to trace out a desired pattern, researchers demonstrated that UV radiation (364 nm) from an argon-ion laser could trace out a test pattern[46] (fig. 3a). It is possible to construct a Mach-Zehnder interferometer with an optimized curvature using this technique.[47] After mounting a test cell containing diacetylene monomer solution on a translation table, a focused UV laser beam passing through the UV transparent surface of the test cell traced the desired paths to form the polymer-based optimized Mach-Zehnder waveguide (fig. 3b).

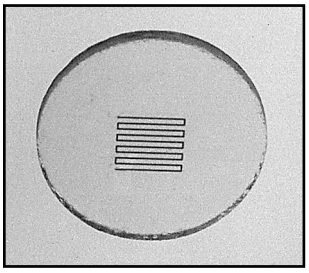

(a)

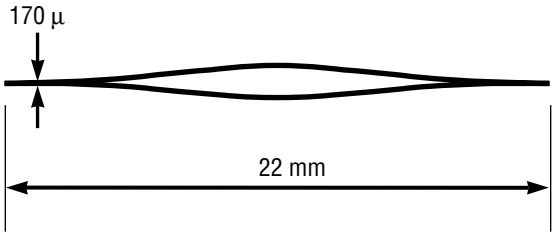

(b)

FIGURE 3.—PDAMNA circuit photodeposited onto UV transparent substrates using the radiation from an argon ion laser: (a) demonstration pattern on a quartz disk, and (b) enlarged image of an actual Mach-Zehnder interferometer on a glass microscope slide.

It has been proposed that NLO thin-film properties may be improved by low-g processing using electrodeposition. Strong candidates for NLO thin-film applications are the polythiophenes (pT). Polymeric thiophenes are attractive materials due to their ease of preparation, stability, and high third-order susceptabilities.[48–52] A simple and convenient method for preparation of pT's is electrochemical oxidation. Earlier microgravity experimentation[53 54] on metal, metal/cermet electrodeposition of Ni provides some microgravity electrodeposition background and raises the possibility of application to improving the quality of pT thin films in low g. Electrodeposition of Ni on an Au substrate in low g often results in the production of an x-ray nondiffracting surface. Similarly deposited cobalt metal does not give this result nor does Ni on a glassy carbon substrate. Further, Co/Ni alloy composition variance during electrodeposition is strongly dependent upon the amount of convection. Similar sensitivities to gravitational influences apparent in inorganics during electrodeposition should arise during electrodeposition of organics.

Electrochemical polymerization deserves thorough investigation for use in fabricating thin film waveguides. NLO films might be prepared on the surface of various substrates during polymerization for the fabrication of devices. This method has been useful in the synthesis of several polymers, in addition to the pT's, such as polypyrrole and polyazulene. The probable existence of thermal and concentration gradients in such dynamic processes suggests an assessment of gravitational influences on film morphologies is justified.

II. GROWTH OF THIN FILMS BY VAPOR DEPOSITION

A. Phthalocyanine Thin Films

This class of materials is an excellent candidate for use in developing NLO devices because of their two-dimensional planar π-conjugation, better chemical and thermal stability than most other organic materials, and ease of derivatizing through peripheral and axial positions (fig. 4). Large[55–64] and ultrafast[52 65 66] third-order nonlinearities have been demonstrated for Pc's. The nature of the central metal atom strongly influences the value of $\chi^{(3)}$. Shirk et al.[56] measured the third-order susceptibility of tetrakis (cumyl phenoxy) Pc's by degenerate four-wave mixing at 1.064 μm. The $\chi^{(3)}_{xxxx}$ values for Pt-Pc (2×10^{-10} esu), lead phtalocyanine (Pb-Pc) (2×10^{-11} esu) were found to be approximately 45 and 5 times that of the metal-free Pc form (4×10^{-12} esu), respectively. Other researchers have shown that $\chi^{(3)}$ of Pc's increase about 15 times by changing the central metal atom from silicon to vanadium[67] and there is also an increase when the central atom is a heavy metal atom such as lead.[68] These positive influences of metal substitution on the third-order optical nonlinearity are attributed to the introduction of low-lying energy states derived from metal-to-ligand and ligand-to-metal charge transfer.[56]

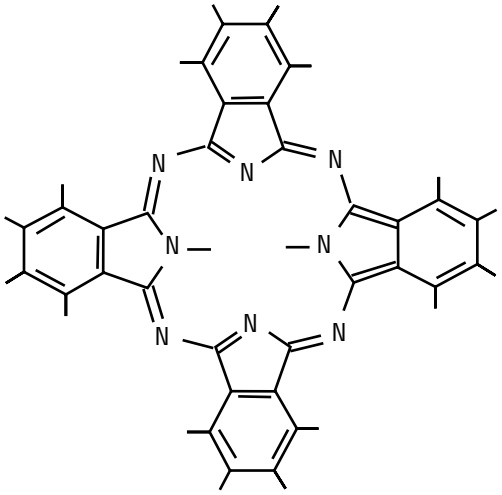

FIGURE 4.—Metal-free Pc (H_2Pc).

Recently, Pc-related compounds have emerged as novel candidates for second-order NLO applications. Sastre et al.[69] measured a β value of $2{,}000 \times 10^{-30}$ for the trinitro-substituted boron subphthalocyanine (subPc) whose structure is shown in figure 5. SubPc's are two-dimensional, 14-π-electron conjugated macrocycles that are composed of three isoindole units containing boron inside. The reported second-order hyperpolarizability for the trinitro derivative is comparable to that of the most efficient linear or dipolar compound.

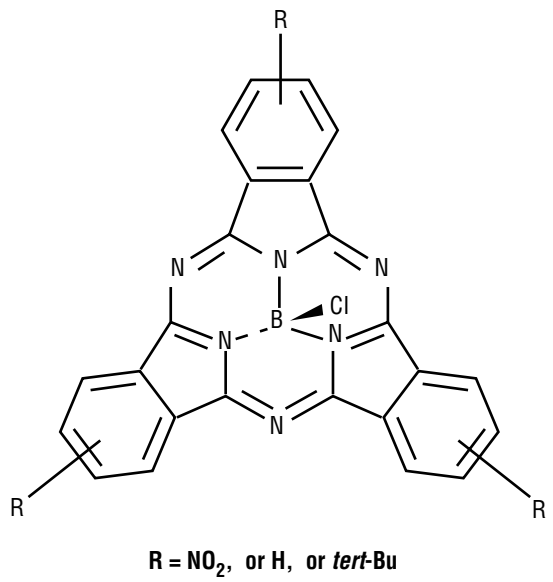

FIGURE 5.—Trinitro-substituted boron subPc.

Difunctional tetraarylporphyrins with nitro groups as electron acceptors and amino groups as electron donors were observed to have a substantial hyperpolarizability by Suslick et al.[70] The β values for cis diamino-dinitro and triamino-mononitro substituted tetraarylporphyrins were 30×10^{-30} esu and 20×10^{-30} esu, respectively. These derivatives were prepared by the partial reduction of the nitro groups of 5, 10, 15, and 20 tetrakis-(p-nitrophenyl) porphyrin. Li et al.[71] measured a relatively large second harmonic generation (SHG: $\chi_{zzz} \sim 2 \times 10^{-8}$ esu) for covalently bound self-assembled monolayer thin films of 5, 10, 15, and 20 tetra (4-pyridyl) 21 H, 23 H-porphine and its derivatives on quartz and silicon <100> substrate having a native oxide layer.

Thin films of Pc for fabrication of waveguides can be obtained by physical vapor transport (PVT) because of their exceptional thermal stability and ease in sublimation. Matsuda et al.[58] observed that Pc with axial ligands, for example, vanadyl phthalocyanine (VOPc), have higher $\chi^{(3)}$ values than most usual unsubstituted Pc. The $\chi^{(3)}$ values of thin films of Pc vacuum deposited at 10^{-4} Pascal onto fused quartz are shown in table 2. The maximum values for the unsubstituted Pc's at 1.9 μm were 1.5×10^{-12} esu for CuPc and 0.8×10^{-12} esu for nickel phthalocyanine (NiPc). In comparison, chloro-indium Pc and vanadyl Pc had $\chi^{(3)}$ values of 1.3×10^{-10} esu and 3×10^{-11} esu, respectively. Ho et al.[55] grew films of chloro-gallium (GaPc-Cl) and fluoro-aluminum (AlPc-F) Pc's onto fused silica flats at 150 °C and 10^{-6} torr. The $\chi^{(3)}$ values for GaPc-Cl and AlPc-F were 5×10^{-11} and 2.5×10^{-11} esu at 1,064 nm for thickness of 1.2 μm and 0.8 μm, respectively.

TABLE 2.—$\chi^{(3)}$ *of vapor-deposited thin films of Pc's measured at a wavelength of* 1.9 μ*m.*[58]

Compound	Film Thickness (μm)	$\chi^3 \times 10^{-12}$ esu (1.9 μm)
(a) Unsubstituted Phthalocyanine		
Copper Phthalocyanine (CuPc)	0.53	1.5
Cobalt Phthalocyanine (CoPc)	0.22	0.76
Nickel Phthalocyanine (NiPc)	0.35	0.80
Platinum Phthalocyanine (PtPc)	0.41	0.60
(b) Unsubstituted Phthalocyanine With Axial Ligands		
Vanadyl Phthalocyanine (VOPc)	0.28	30
Titanyl Phthalocyanine (TiOPc)	0.26	27
Chloro-aluminum Phthalocyanine (ClAlPc)	0.26	15
Chloro-indium Phthalocyanine (ClInPc)	0.14	130

Wada et al.[72] measured a $\chi^{(3)}$ of 1.85×10^{-10} esu at 1.907 μm for a 51.4-nm-thick film of VOPc vacuum deposited onto quartz. The $\chi^{(3)}$ values for two different phases in vanadyl and titanyl phthalocyanines (TiOPc's) were measured by optical third-harmonic generation at wavelengths of 1,543 nm and 1,907 nm by Hosoda et al.[73] The transformation of as-prepared Pc films from phase I to phase II was performed by thermal annealing and was accompanied by a red shift in absorption spectra and an increase in $\chi^{(3)}$ values of 2–3 times. $\chi^{(3)}$ values for as-prepared films of VOPc and TiOPc were 3.8×10^{-11} esu and 10^{-11} esu, while the annealed films had values of 8.1×10^{-11} esu and 4.6×10^{-11} esu, respectively.

Recently, relatively strong second-harmonic generation (SHG) was reported for vacuum-deposited CuPc films which possess inversion symmetry. Chollet et al.[74] measured a $d_{eff} \approx 2\times10^{-19}$ esu at 1.064 μm fundamental wavelength for films with thicknesses ranging from 50 to 500 nm that were prepared at a pressure of 10^{-6} torr and source temperature of 120 °C. The films were homogeneous and partly oriented with a relatively large distribution of molecular axes, oriented almost perpendicular to the substrate. This order was confirmed by SHG measurements. SHG in the films was attributed to quadrupolar or dipolar origins. Kumagai et al.[75] prepared 40- to 2,000-Å-thick films at a pressure of 5×10^{-6} torr and obtained $\chi_{zyy} = 4\times10^{-8}$ esu at 1.06 μm fundamental wavelength, which is a quarter of the value for $LiNbO_3$. They proposed a mechanism in which an asymmetric crystal field acting perpendicular to the surface makes each CuPc molecule capable of SHG. Yamada et al.[76] performed in situ observation of SHG from CuPc films during vacuum evaporation on glass at a pressure of 1.5×10^{-5} torr and a rate of 1.2 nm/min. Thickness dependence on SHG was compared with calculations based on electric dipole, electric quadrupole, and magnetic dipole mechanism to clarify the origin of SHG activity. Based on the comparison, SHG was ascribed to electric quadrupolar or, preferably, magnetic dipolar origin.

The research of Debe et al.[77–79] indicates that better quality organic thin films for use in NLO devices might be obtained by closed-cell PVT in microgravity. In the PVT process, the source material is sublimed in an inert gas and allowed to convect or diffuse down a thermal gradient and to ultimately condense at a crystal or thin film growth interface.[77] The advantage of thin film growth in microgravity is that it provides the opportunity to eliminate buoyancy-driven convection. Recent reports[77–79] of the space shuttle mission STS–51 of August/September 1985 include results of experiments in which CuPc was epitaxially deposited, by PVT, onto highly oriented seed films of metal-free Pc (H_2Pc). The substrate was a 1.4-cm-diameter solid copper disc.

The PVT of organic solids apparatus used to grow CuPc thin films consisted of nine identical metal/Pyrex ampoules housed within its own heater assembly and vacuum insulation cell.[77 78 80] Films were grown in 1.7-cm-diameter by 7.5-cm-long Pyrex tubes that were placed within resistance wire-wound heaters which induced a nonlinear axial thermal gradient. The growth ampoules were filled primarily with CO_2, H_2, the buffer gas Xe, or He and then either N_2 or CO as the next most abundant component. A computer-controlled heater maintained the hot end of the ampoule, containing the source, at 400 °C for 4 hours after the cruise temperature was reached. The substrate was maintained at a temperature of 70 °C by a heat pipe.

The substrate seed film was prepared by vacuum sublimation of H_2Pc onto a copper disc at a temperature range known to produce highly oriented films. A metal-free Pc film with a thickness of 1,100 ± 50 Å was grown at a deposition rate of 70 Å/min. The substrate was held at a temperature of 5 to 10 °C and the source-to-substrate distance was 16 cm. Debe has shown that highly oriented films of H_2Pc are obtained when the substrate temperature range is approximately 5±5 °C.[80] Before starting the growth process, the source material was outgassed by slowly increasing the temperature of the hot zone. After ~ 2 hours of “soaking,” the temperature was increased to cause the H_2Pc material to deposit on the copper substrate at a pressure of about 5×10^{-6} torr.

Microgravity-grown CuPc films had several desirable features which indicate that the growth of organic films in low-g may result in better quality films for NLO applications. For example, results of analysis by visual photography, bright field and differential interference contrast microscopy, scanning ellipsometry, visible reflection spectroscopy, and direct interferometric phase contrast microscopy imply that the space-grown films were radially more uniform and homogeneous, and an order of magnitude smoother over the submillimeter to submicron scale range.[77] Results of analysis involving the use of external reflection-absorption infrared (IR) spectroscopy, grazing incidence x-ray diffraction, and visible-near IR reflection-absorption spectroscopy infer that the microgravity-grown films are more highly uniaxially oriented and the films were found to consist predominantly of crystalline domains of a previously unknown polymorphic form of CuPc.[78] In addition, scanning electron microscopy analysis revealed that there was a distinctly different microstructure in the center of the space-grown films and that the circular perimeters of the microgravity-grown films had microstructure much like that of the ground control films in both their center and edge regions.[79]

As stated earlier in the chapter, electric field poling of polymers containing the nonlinear chromophore may be used to induce macroscopic asymmetry. However, in the case of the ring-

structured macromolecule, phthalocyanine, poling is not generally an option to achieve ordering in deposited films. It is therefore beneficial to achieve, if possible, self-assembly to induce required asymmetry by other means. Whenever self-assembly might occur in molecules not prone to poling, exploitation of conditions favorable toward asymmetry could prove beneficial. In the case of Pc, for example, $\chi^{(3)}$ enhancement and possible $\chi^{(2)}$, inducement might result from self-assembly. Vapor-deposited H_2Pc have demonstrated some potentially interesting NLO properties. Researchers report these films to be randomly oriented when processing occurs in 1-g (fig. 6a).[43 44 77–80] From microgravity processing, CuPc films epitaxially deposited onto H_2Pc films are highly oriented and densely packed (fig. 6b). Abdeldayem et al.[81] recently observed intrinsic optical bistability in vapor-deposited thin films of metal-free Pc, ranging in thickness from 40 to 800 nm, using continuous wave (CW) and chopped He-Ne lasers at 633 nm. Source and substrate temperatures were maintained at 300 °C and 5 °C, respectively, while vapor vacuum deposition occurred at 10^{-6} torr onto quartz disks. Bistability in the film was attributed to changes in the level of absorption and refractive index caused by thermal excitation. This nonlinear effect could improve dramatically in highly oriented microgravity processed films.

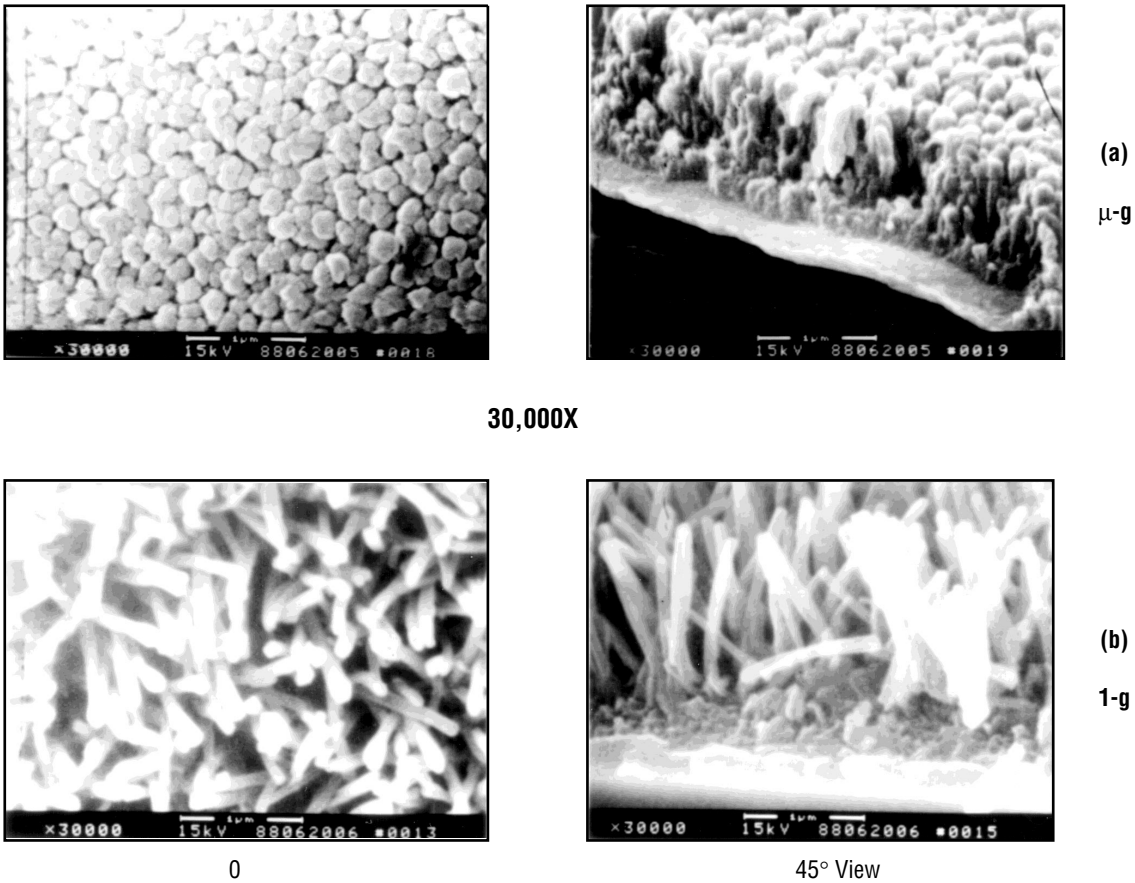

FIGURE 6.—CuPc films epitaxially vapor-deposited onto copper substrate: (a) μ-g deposition of CuPc epilayer, and (b) 1-g deposition of CuPc epilayer (courtesy of 3M Corporation).

For a discussion of optical bistability, we first recognize that the absorption spectrum in the visible region shows a strong maximum at 626 nm. In one experiment,[81] the CW He-Ne (632.8 nm) laser at a fixed input power of ~30 mW was focused on a 230-nm-thick film. The beam transmission increased temporally over a period of nearly 12 hours as shown in figure 7a. The nearly straight line of figure 7b is a fraction of the input power for monitoring laser stability. Fitting the transmission data to a single exponential (the solid line) gave a rise time of ~2.2 hours to reach a steady state.

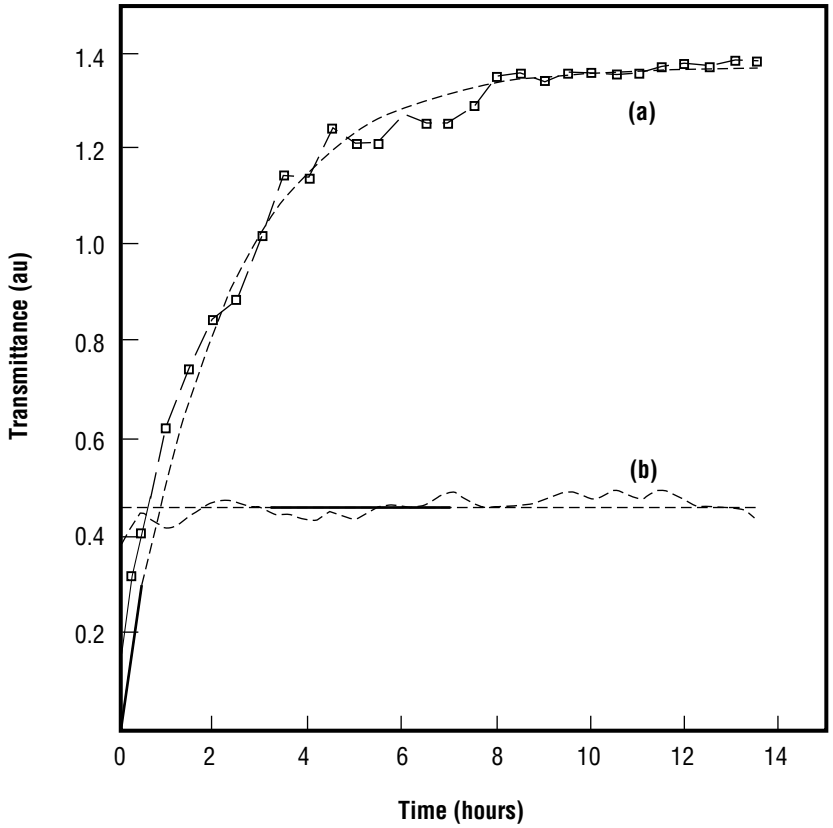

FIGURE 7.—(a) Time-dependent transmittance through a metal-free Pc film (230-nm-thick), using a CW He-Ne laser at 632.8 nm and 30 mW power. The dotted curve represents the experimental data, while the solid line represents a single exponential theoretical fit. (b) The dotted line represents laser stability throughout the experiment, while the solid line is the corresponding straight-line fit.

The temporal transmission effect in the film can be explained by the following sequence: (a) The initial low transmission of the beam through the film can be attributed to a strong absorption of the beam which generates free electrons and holes; (b) these free charges relax to excitonic states[82] and release their excess energy as heat to the system at the focal point; (c) the build-up of localized heating at the focus reduces absorption of the He-Ne radiation, causing saturation of absorption. This factor is in

agreement with the results of a separate experiment to measure the sample's absorption at a temperature elevated above room temperature by a water bath. Such reduction in absorption allows more transmission to occur with time.

Investigation of the bistability of metal-free Pc films of 833-nm thickness used a chopped He-Ne 632.8-nm laser beam at frequencies ranging from 100 to 750 Hz. The film was positioned on a micrometer stage, at the lens focus, and transversely translated in and out of the beam alternately to record intensity input and film transmittance. A Hewlett Packard (HP) digitizing oscilloscope, model 54120B, recorded the input and the transmitted pulse with an HP plotter, model 7470A (fig. 8). The nonsymmetrical shape of the transmitted pulses (fig. 8b) indicated the presence of intrinsic bistability in metal-free Pc. Figure 8c depicts typical bistable switching, constructed from the transmitted pulse. The switching power of ~ 0.33 mW per pulse in combination with a pulse duration of 1.37-ms recovery time yields a very low switching energy of ~ 0.45 nJ. Observation of bistability was repetitive in the same film using a CW He-Ne laser as shown in figure 9 for different timespans between successive points.

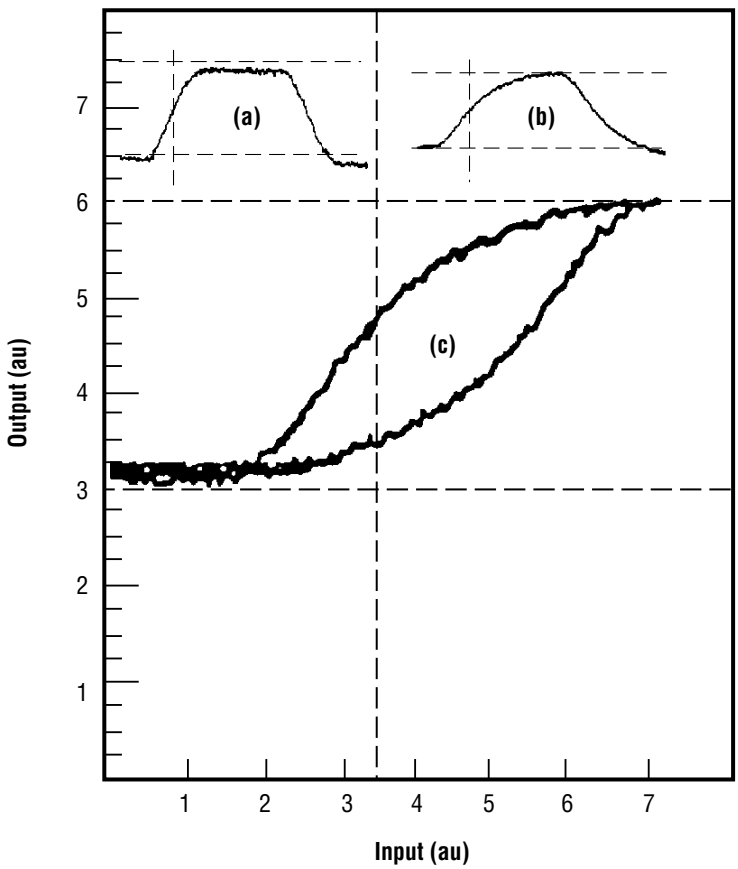

FIGURE 8.—The bistability loop of an 833-nm metal-free Pc film using a chopped CW He-Ne laser at 632.8 nm: (a) the input pulse, (b) the transmitted pulse, and (c) hysteresis switching constructed from (b).

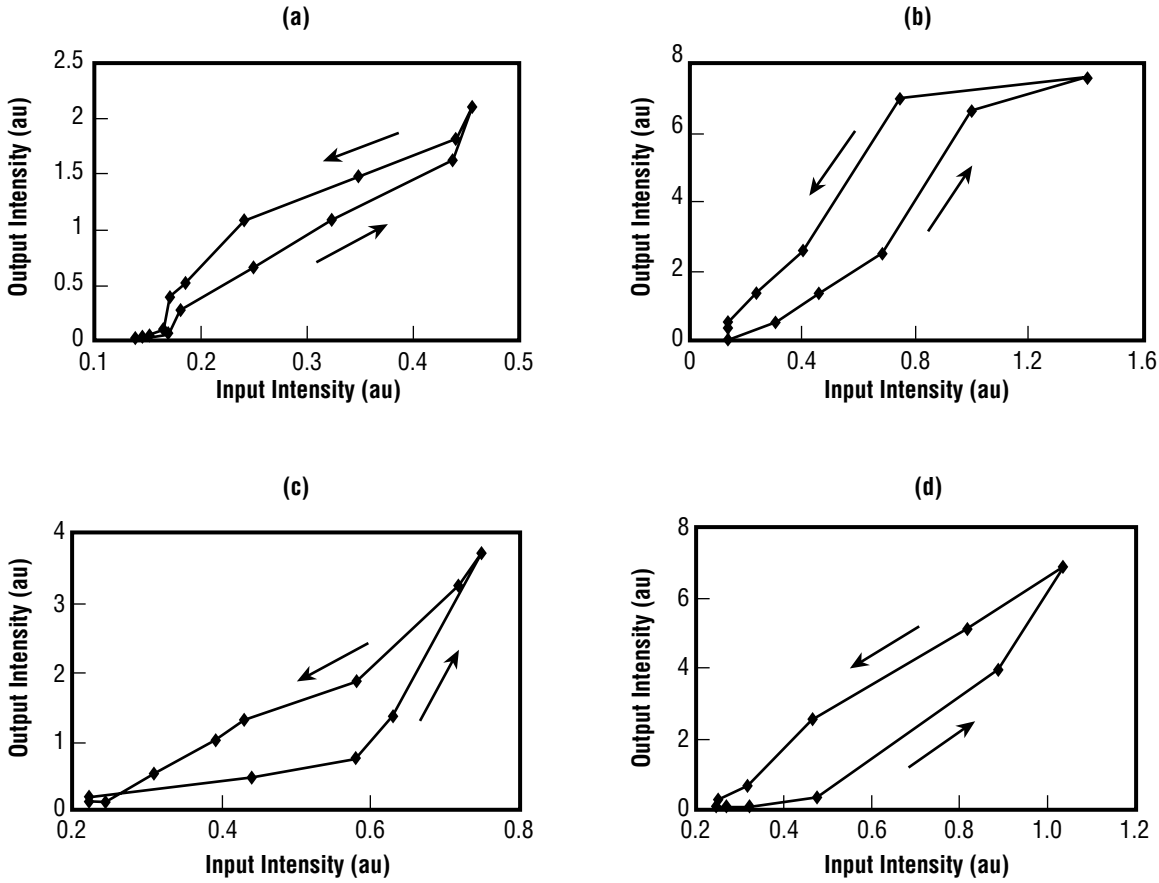

FIGURE 9.—The bistability loops for different timespans of a metal-free Pc film of 232.5-nm thickness using a CW He-Ne laser. Timespans between successive points are (a) 3.84 sec, (b) 10 sec, (c) 342 sec, and (d) 1,800 sec. (a) Shows the least prominent bistability loop while (b), (c), and (d) show a minimal effect of the timespan between points.

A thinner film, 230 nm, also demonstrated saturation of absorption at the same He-Ne laser frequency. Figure 10 illustrates the experimental data recording absorption by a 230-nm-thick film and the theoretical curve-fit assuming Bloch-type saturable absorption with negligible scattering losses[83]

$$a(I)L = [a_o L/(1 + I/I_s)] \tag{1}$$

where I_s is the threshold power of the saturation, L is the thickness of the sample, and a_o is the linear absorption coefficient. The saturation intensity, estimated from the theoretical fit, is

$$I_s \sim 2.0 \times 10^4 \text{ W/cm}^2 \ .$$

Modeling Pc as a three-level system, a molecule in the ground state at saturation absorbs light at a rate

$$1/t = s_o I_s / hf \tag{2}$$

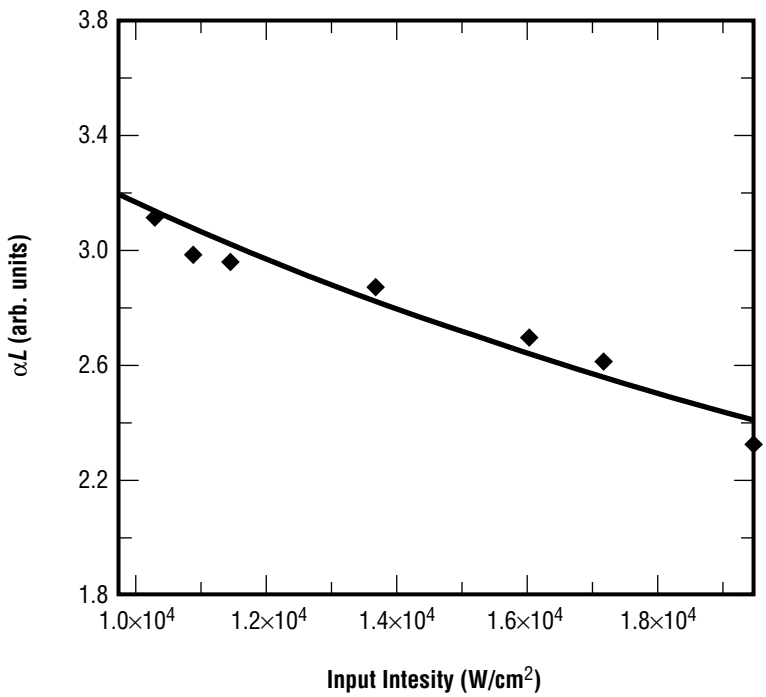

FIGURE 10.—Experimental and theoretical fitting of saturable absorption of a metal-free Pc film (232.5-nm thickness) at 632.8 nm from a CW He-Ne laser. The corresponding saturation intensity is 19.8×10^3 W/cm^2.

where t is the decay time of the excited triplet state, I_s is the saturation intensity, s_o is the absorption cross section of the groundstate, and hf is the energy of the incident photon. From the measurements of the fall time of 1.0756 ms at 245 Hz in figure 6b, the absorption cross section was estimated[84] to be on the order of $\sim2.4\times10^{-17}$ cm^2.

The estimated third-order nonlinear susceptibility measurements by four-wave mixing using pulsed Nd:YAG laser at 532 nm was on the order of 10^{-8} esu. This relatively large value is attributed to both resonant as well as thermal mechanisms that might be present in the system at this wavelength.

B. Polydiacetylene Thin Films

1. Second and Third-Order NLO Properties of PDA's

PDA's (fig. 11) are highly conjugated organic polymers that are of considerable interest because of their unique chemical, optical, and electronic properties.[85–88] This class of polymers has received extensive attention as organic conductors and semiconductors, as well as NLO materials. The high mobility of the π-electrons in the polymer backbone allows them to have large optical/electrical susceptibilities with fast response times. They can be highly ordered, even crystalline, which is important for optimizing their electronic and optical properties, and they can readily be formed into thin films, which is the preferred form for many applications. The physical, chemical, and mechanical

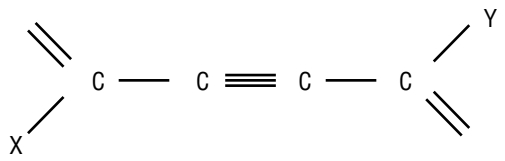

FIGURE 11.—Structure of PDA repeat unit.

properties of PDA's can be varied by changing the functionality of the side groups, thereby making it possible to tailor their properties to meet specific needs. Thus, there is a great deal of interest in the use of these polymers for technological applications.

PDA's are among the best known third-order NLO materials, and there has been considerable investigation over the past 20 years into their properties. Single crystals of poly (2,4-hexadiyne-1,6-ditosylate), also known as PTS, possess one of the largest (possibly the largest) nonresonant third-order optical nonlinearities ever measured, on the order of 10^{-9} esu.[89] The third-order NLO properties of numerous other PDA crystals and thin films have also been determined. Typical $\chi^{(3)}$ values for PDA's range from 10^{-7} to 10^{-12} esu, depending on the degree of resonance enhancement and other factors. Both theoretical and experimental results have determined that the $\chi^{(3)}$ value is approximately 100 times greater along the PDA backbone than perpendicular to it, demonstrating the effect of the conjugated π-electron system. Because the origin of the nonlinearity is electronic, they can have very fast response times, on the order of femtoseconds.

More recently, PDA's have been investigated as potential second-order NLO materials. Theoretical calculations have indicated that certain PDA's could possess extremely high second-order NLO susceptibilities; e.g., molecular hyperpolarizabilities on the order of $1{,}000\times10^{-30}$ esu.[90] In order to make use of this second-order nonlinearity, it is necessary to orient the polymers into acentric structures, either crystals or thin films. This is not trivial; many compounds which have desirable properties at the molecular level tend to orient themselves centrosymetrically in the bulk to minimize electrostatic interactions.

SHG has been observed from certain asymmetrical liquid-crystalline diacetylene monomers (although, interestingly, not from the corresponding polymers)[91] from both LB and self-assembled PDA monolayer and multilayers[92 93] and even from a spin-coated PDA film.[94] Lastly, powder SHG efficiencies comparable to that of 2-methyl-4-nitroaniline (MNA) have been obtained from vapor-deposited polycrystalline films of a PDA possessing MNA as a side group.[90] If the crystallites are partially aligned by growing the films quasi-epitaxially onto prealigned poly (tetrafluoroethylene) substrates, the SHG efficiency increases by almost one order of magnitude.

2. Potential Benefits of Microgravity Processing

Optical applications require the formation of high quality thin PDA films; i.e., films possessing minimal defects such as impurities, inhomogeneities, light-scattering centers, and so forth. The standard

techniques for obtaining PDA thin films involve the growth of crystalline diacetylene monomer films or the deposition of LB films, followed by topochemical polymerization of these films in the solid state to yield ordered PDA films. This ability to undergo solid-state polymerization is a very intriguing property of diacetylenes; in principle, one can start with a single crystal monomer and obtain a single crystal polymer.[7 95] However, the process is not trivial; the formation of high-quality, crystalline diacetylene monomer films or LB films can be very tedious and difficult, and, furthermore, by no means do all monomers polymerize readily in the solid state.[8] Achieving high-quality PDA films requires the growth of high quality diacetylene monomer films, which are then topochemically polymerized. A commonly employed technique for obtaining diacetylene monomer films is vapor deposition. One of the chief limitations to vapor deposition of high quality monomer films; e.g, single crystalline films with good molecular orientation and few defects, has been a lack of understanding of how the processing conditions affect monomer film growth. It is certainly well known that parameters such as temperature, pressure, concentration, and so forth can affect vapor transport processes. One parameter which is often tacitly ignored is the influence of gravity. However, the effects of gravity, such as buoyancy-driven convection, can greatly influence heat and mass transport during the growth process, and thereby influence all of the aforementioned growth parameters. Thus discerning the effects of gravity (or the lack thereof) could play a critical role in optimizing the growth of high-quality PDA films by vapor deposition.

One method of assessing convection in a gas phase is to perform the computation at low pressure to relieve the need for specific materials constants. It is important to note that buoyancy effects are possible only if the molecular mean free path is short enough relative to cell dimensions such that molecular flows are not in the free molecular flow regime. A mathematical model has been developed to determine buoyancy-driven heat transfer in an ideal gas under a variety of orientations relative to gravitational accelerations.[96] The model demonstrates that convection can occur at total pressures as low as 10^{-2} mm Hg in cells having relatively high length-to-width ratios. A preliminary experimental test of the model involved deposition of the diacetylene monomer, 6-(2-methyl-4-nitroanilino)-2, 4 hexadiyn-1-ol (DAMNA) (fig. 12), at an evacuation pressure of 10^{-2} mm Hg.

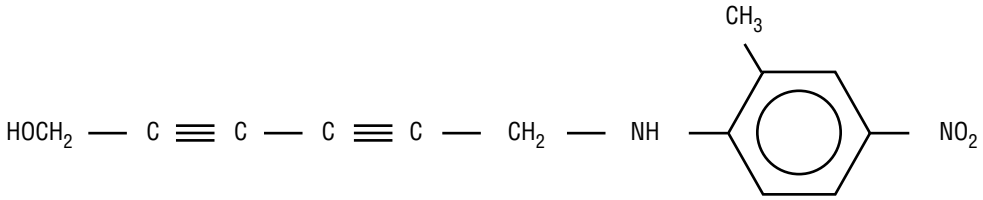

FIGURE 12.—Diacetylene monomer, DAMNA.

The deposition of DAMNA by PVT was of 30-min duration. Cell dimensions were the same as those depicted in figure 13 with source temperature of 120 °C and sink temperature of 30 °C. The evacuation pressure reached a minimum in the presence of DAMNA (10^{-2} mm Hg), and was significantly lower in the absence of DAMNA. It is probable that the DAMNA vapor pressure is equal to, or greater than, the evacuation pressure of 10^{-2} mm Hg. From a different study, the measured vapor pressure of 4-N,N-dimethylamino- 4′-nitrostilbene (DANS) at 120 °C was reportedly 0.374 mm.[97]

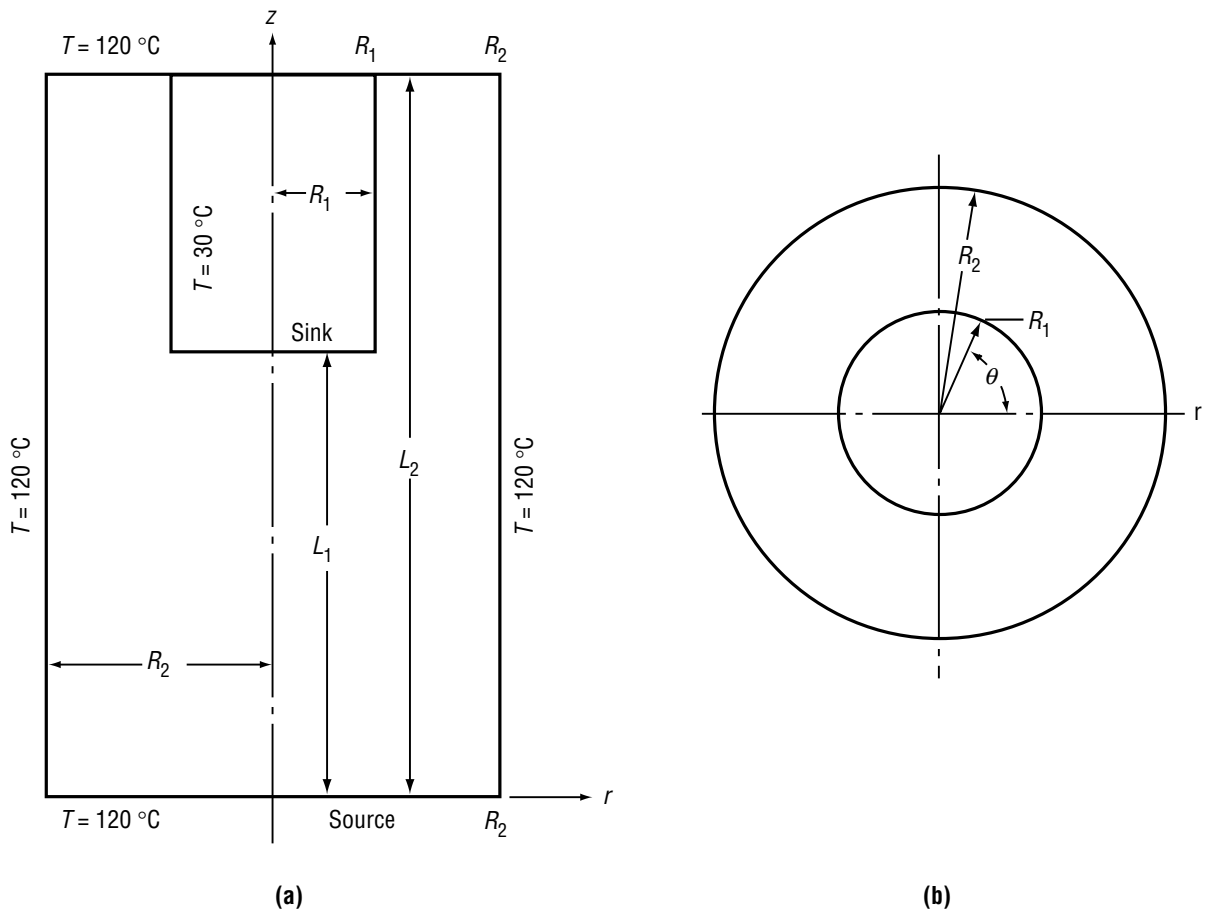

FIGURE 13.—Vapor deposition cell for PVT of DAMNA.

This is a relatively large organic molecule having a molecular weight of 211 g/mole as compared to DAMNA with a molecular weight of 247 g/mole. Considering structural and size similarities, we may approximate similarities in vapor pressure. Indeed, heptadecanol (molecular weight = 256.5 g/mole), also an alcohol with possible hydrogen bonding in its condensed phases such as expected of DAMNA, has a vapor pressure of 10^{-1} mm at 120 °C.[98] There is no reason to expect DAMNA to differ drastically from these measured vapor pressures, and we may approximate that the vessel evacuation pressure minimum is largely due to the vapor pressure of DAMNA.

Using physical material parameters of air, a series of time steps demonstrates the development of flow and temperature profiles in an ideal gas. These profiles are driven by the specified temperatures with no mass fluxes (there are no subliming or condensing masses in this model) in a vessel as specified in figure 13. Computations show that in unit gravity it is possible that vapor deposition occurs by transport through an axisymmetric circulating flow pattern when applying heat to the bottom of a vertically positioned vessel. In the case where heating of the reaction vessel occurs from the top, deposition of vapor does not normally occur by convection due to a stable stratified medium. When vapor deposition occurs in vessels heated at the bottom, but oriented relative to the gravity vector between these two extremes, horizontal thermal gradients induce a complicated asymmetric flow pattern.

Comparison of figures 14 and 15 and figures 14 and 16 show the differences in induced flow fields in the $\theta = 0°–180°$ and $\theta = 90°–270°$ planes, respectively, driven by vertical and tilted cavities. There are two recirculation flows generated with centers at $(r_c, z_c) = (\pm 1.90, 2.7)$ cm and at $(r_c, z_c) = (\pm 0.8, 3.2)$ cm for flows induced by vertical and tilted orientations, respectively. For the vertical orientation, the flow depicted in figure 14 is axisymmetric, hence also representative of flows in the $\theta = 90°–270°$ plane. The flows are upward along the surface of the outer cylinder and downward from the central column. These are Benard-type flows driven by counter-rotating cells (clockwise on the left and counter-clockwise on the right) due to an incipient instability in the narrow cylindrical cell cavity. There is no critical Rayleigh number for convection which assumes an infinite extent of the cell width. For the tilted cell, a resultant asymmetric flow in the $\theta = 0°–180°$ plane approaches an antisymmetric flow profile resulting from differential heating between vertical and opposite walls of a cavity. That is, an incipient instability causes heat to flow along the bottom surface (now tilted upward), upward along the side wall, along the cold surface (downward), and downward along the other side wall. The two recirculation flows for this orientation appear in the $\theta = 90°–270°$ plane (fig. 16). There is an

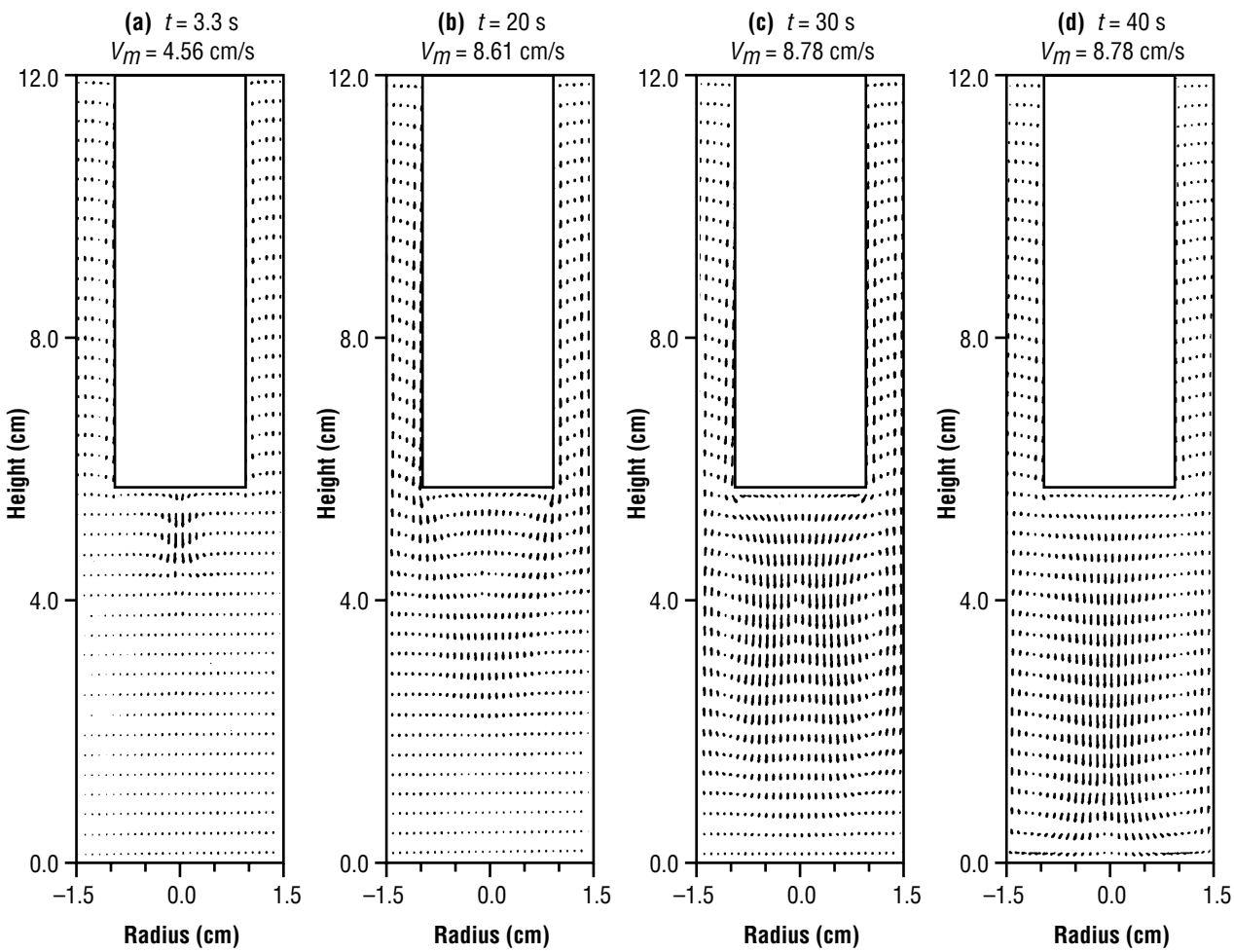

FIGURE 14.—Axisymmetric flow in the $\theta = 0°–180°$ plane in cell in which deposition occurs with cell oriented vertically.

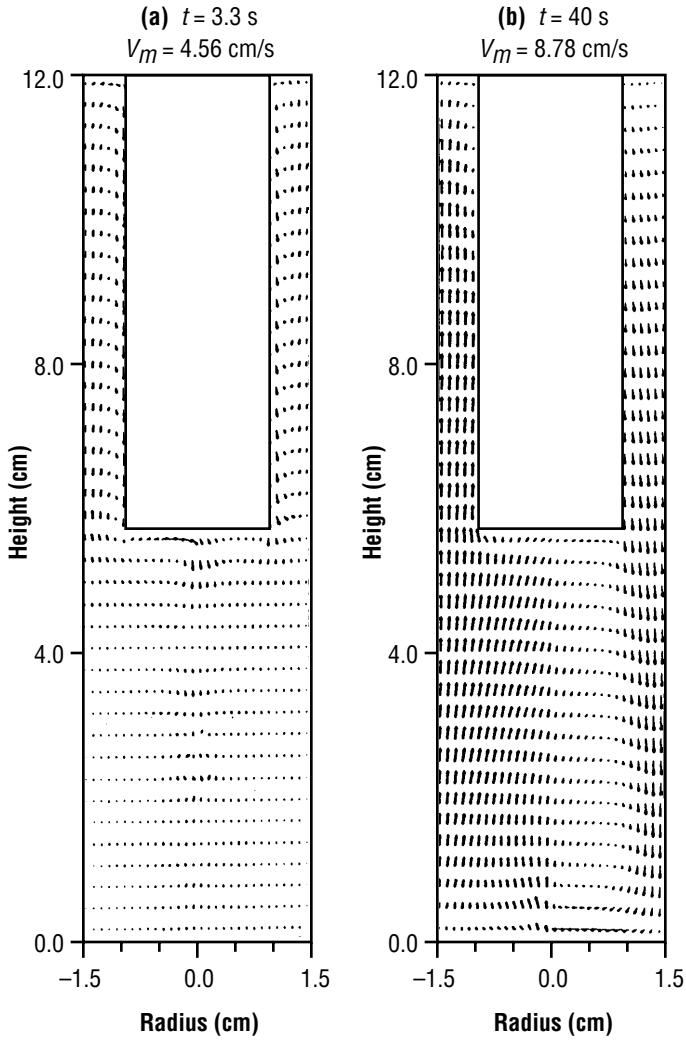

FIGURE 15.—Flow in the $\theta = 0°–180°$ plane in cell in which deposition occurs with cell tilted 45° to vertical axis.

upward flow from the bottom surface of the outer cylinder transporting heat toward the bottom surface of the central column with downward flows on the outside walls (clockwise on the right and counter-clockwise on the left). This asymmetric three-dimensional flow profile is quite complex and represents a greater degree of convection in the cell cavity for the tilted orientation than for the vertical orientation. The model material parameters for air predict the effect of kinematic viscosity to be of the same order as thermal diffusivity, which is the case for Prandtl number ~1 fluids.[99] The classical heat capacity for a gaseous molecule, such as DAMNA, with its large number of vibrational degrees of freedom, is only achieved at high temperatures. That is, the heat capacity of DAMNA will approach that of a diatomic molecule such as the major components of air, since its vibrational modes are unable to store energy at these relatively low temperatures. The thermal diffusivity approximation using air data is, therefore, a fair one, assuming similar heat conduction coefficients. In the classical limit, the higher heat capacity would yield $Pr >> 1$. Because an ideal heat capacity approximation is an overestimate at the operating temperatures, deviation from ideal behavior causes $Pr \sim 1$, closer to that of air. Without actual data for

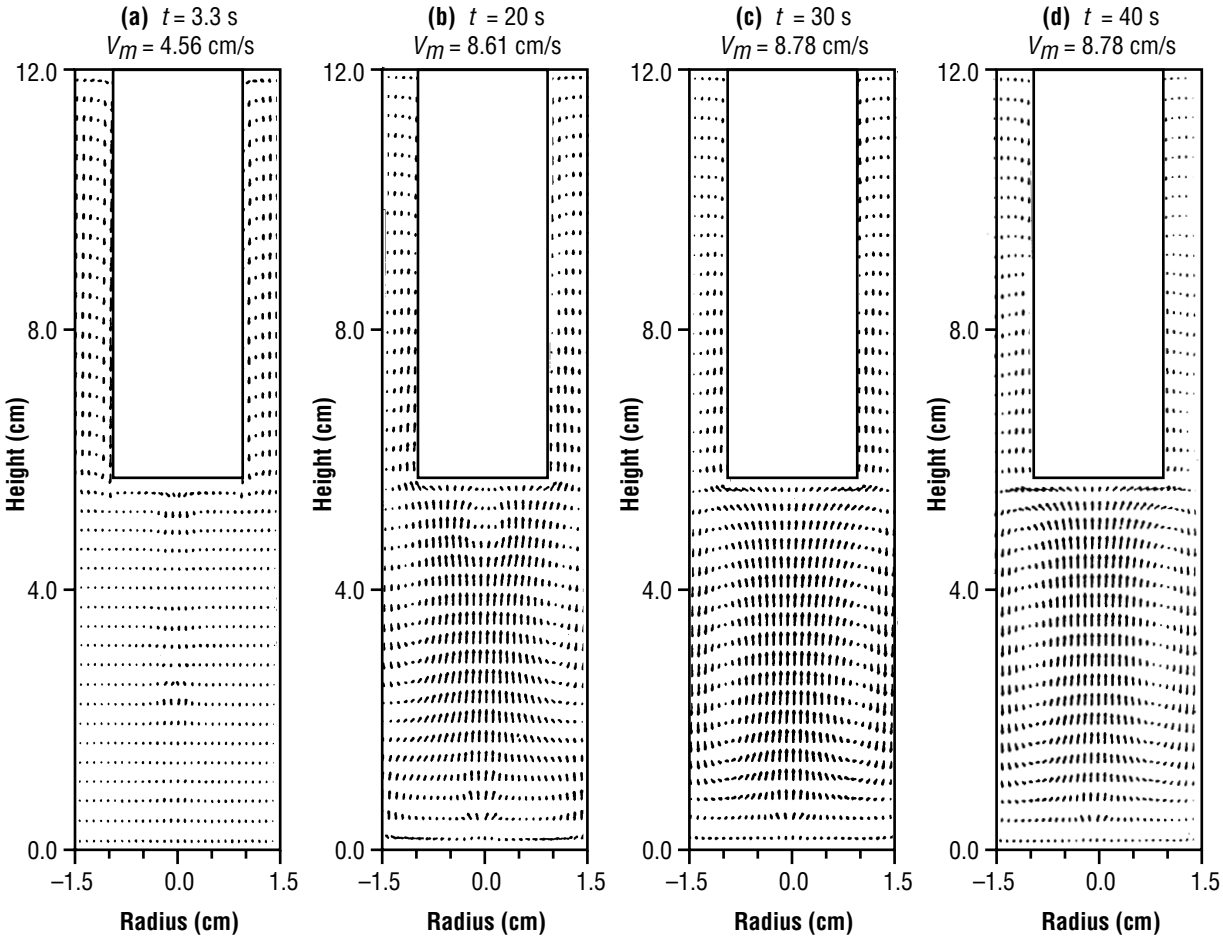

FIGURE 16.—Flow in the θ = 90°–270° plane in cell in which deposition occurs with cell tilted 45° to vertical axis.

DAMNA, we are left with experimental data from the low operating pressures and temperatures to compare with modeling estimates. Close agreement between experiment and the model would indicate that DAMNA at these pressures indeed approximates an ideal gas with the appropriate deviations which tend toward validation of the use of air physical constants. Furthermore, the constant heat flux provided by the circulating bath is a factor in neutralizing thermal effects specific to individual molecules.

Experimentally, it is helpful to utilize Beer-Lambert's relationship for transmission of radiation through a medium to test gravitationally sensitive flow pattern predictions.[96] We would expect that the flow pattern in figure 16 (cell tilted at 45° relative to gravity vector) would affect film quality over most of the deposition surface differently than the flow pattern depicted in figure 14 (cell oriented vertically). Preliminary experiment suggests this to be the case with respect to film thickness. The Beer-Lambert law relative to film thickness can be written

$$I = I_o \varepsilon^{-\alpha \ell} \tag{3}$$

where I_o is incident radiation intensity; I is the reduced radiation intensity after passing through the film; α a proportionality constant containing the molar absorption coefficient, ε, and concentration of absorber; and ℓ is film thickness. The molar absorption coefficient represents a molar cross section for absorption. The greater the cross section of the molecule for absorption and absorber concentration, the greater the attenuation of the intensity of the beam. Likewise, film thickness, ℓ also attenuates the beam intensity accordingly. The ratio I/I_o is a measure of beam transmittance, T. If increased convection yields greater film thickness, we would expect a larger intensity in the absorption bands of films deposited in cells tilted at 45° over those where deposition occurred in cells positioned vertically. We may define the dimensionless product $A = -\alpha\ell$ as absorbance which incorporates all of the contributors to beam attenuation. Since the nature of the material, DAMNA, and concentration (pure material) are identical in both cases, then absorbance is only a function of film thickness. Figure 17a is a wavelength scan in the range 190 to 820 nm of a vertically deposited film, and figure 17b is that of an obliquely deposited film. Table 3 contains representative absorbance intensities from scanning an approximately 1-cm-diameter spot in similar vicinities of films formed during vapor deposition in vertically and obliquely oriented cells. Visually, the films from the obliquely oriented cells are a deeper yellow color than those from vertically oriented cells. We qualitatively assume generally thicker films from the relative appearances. The surfaces of these monomer films are translucent and microcrystalline. At the present time, it is also preferable for us to discuss relative film thickness from beam attenuation in qualitative terms (although more quantitative than visual observation) while observing that the spectroscopic irradiation spot sizes are large enough to average over about 50 percent of the film surfaces. The same relative result occurred in that beam attenuation was greater at each maximum absorbance wavelength repeatedly. We may consider the data in table 3 a qualitative representation of a consistent result.

In keeping with the assumptions, the mathematical model correctly predicts qualitative differences in film properties between vertically and obliquely oriented cells; i.e., more convection in cells having the tilted orientation is apparently responsible for correspondingly greater film thickness.

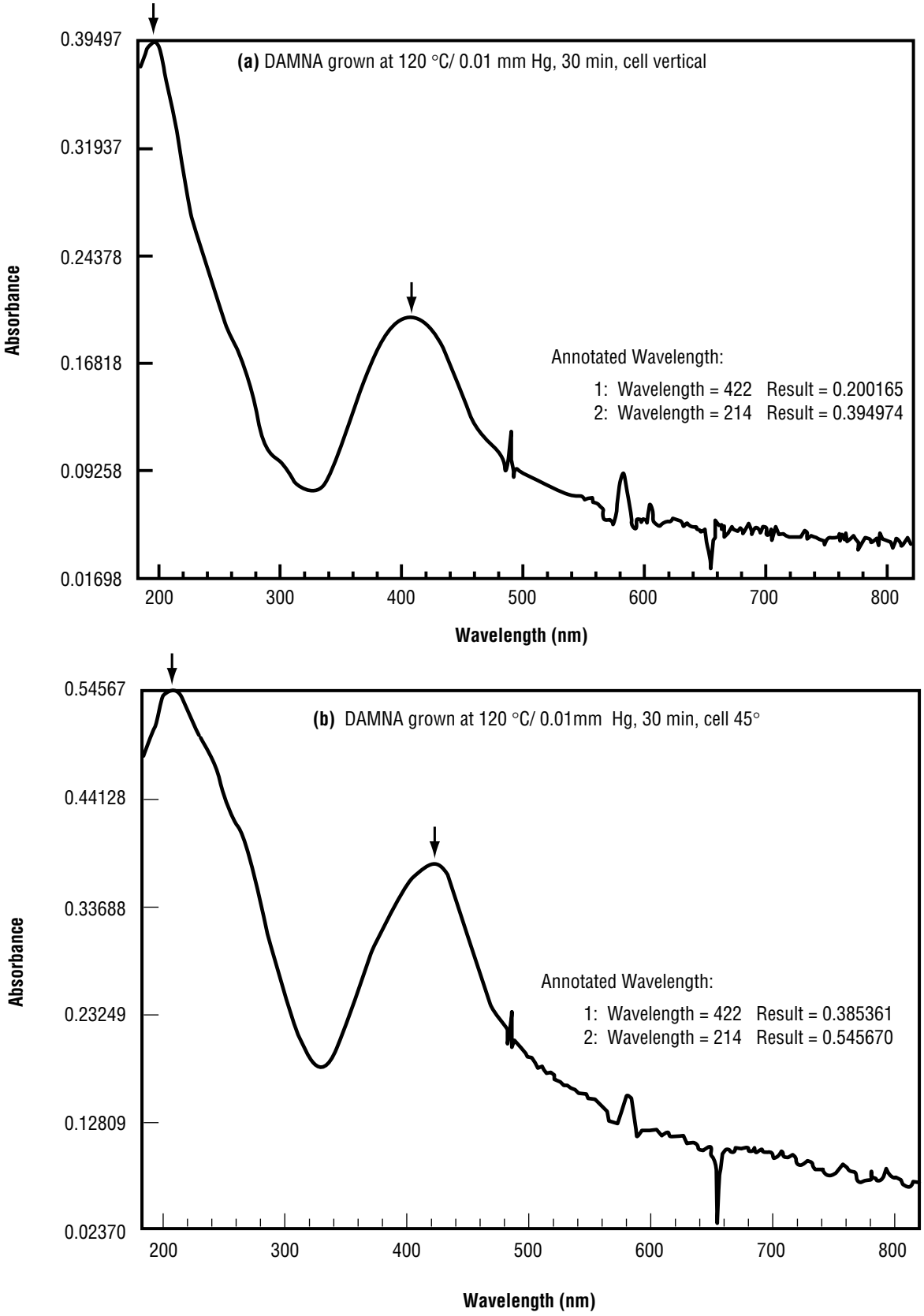

FIGURE 17.—Absorbance as function of wavelength for vapor-deposited film after 30 minutes of deposition for (a) a vertically oriented cell, and (b) a tilted cell.

TABLE 3.— *Representative absorbance intensities from scanning an approximately 1-cm-diameter spot in similar vicinities of DAMNA films formed during vapor deposition.*

λ (nm)	A_{max} (cell vertical film)	A_{max} (cell tilted film)
422	0.200	0.385
214	0.395	0.546

III. GROWTH OF THIN FILMS BY SOLUTION PROCESSES

A. Ultraviolet Solution Polymerization

1. Polydiacetylene Films

Recently, a novel process has been discovered for the formation of thin amorphous PDA films using photodeposition from monomer solutions onto transparent substrates.[33 45 46 90] Specifically, polymeric films were directly synthesized from a diacetylene monomer, DAMNA (fig. 12), derived from 2-methyl-4-nitroaniline (MNA) that only sluggishly polymerizes when the crystalline monomer is irradiated.[100] This compound was one of several asymmetric diacetylenes that were first studied extensively for their optical and electronic properties by Garito and coworkers in the late 1970's; however, their investigations did not include behavior in solution.[101 102] It was found that thin polymerized DAMNA (PDAMNA) films can be obtained readily from solutions of DAMNA in 1,2-dichloroethane by irradiation with long wavelength UV light through a quartz or glass window, which serves as the substrate. This simple straightforward process yields transparent films with thickness on the order of a micrometer.

Despite the considerable volume of literature available on diacetylenes and PDA's, this solution-state photodeposition reaction has never been reported. Thus many of the parameters controlling the efficacy of the process are not yet known. The basic idea is quite straightforward; the diacetylene monomer solution is irradiated through a UV transparent substrate and a thin PDA film results. To date, several diacetylene monomers have been tested and found to be capable of photodeposition of polymeric films from solution.

Special chambers were constructed for carrying out the reaction and obtaining thin films on small round substrate disks (fig. 18). To obtain a PDAMNA thin film, a solution of DAMNA in 1,2-dichloroethane (approximately 2.5 mg/ml = 0.01 moles/L) is placed inside the chamber, and the chamber is then irradiated through the substrate with long wavelength UV light (365 nm). The thickness of the resulting PDAMNA film depends on the duration of exposure and the intensity of the UV source. After the photodeposition is complete, the monomer solution, which now also contains suspended particles of precipitated polymer, is removed from the growth chamber. The substrate, now coated on one side with the PDAMNA film, is then removed, washed with 1,2-dichloroethane, and dried.

Thin PDAMNA films obtained in this manner are transparent, glassy yellow-orange in appearance, suggesting an amorphous nature. Both refractive index measurements and electron beam diffraction studies indeed indicate that the films are amorphous. The films are insoluble in organic solvents, although solvents such as acetone can cause them to peel off of the substrate. Even concentrated sulfuric acid does not dissolve the films; they turn brown, shrivel, and peel off of the substrate, but do not dissolve, even after several weeks. In contrast, the PDAMNA powder precipitated from the bulk solution is soluble in solvents such as acetone and dimethylsulfoxide (DMSO).

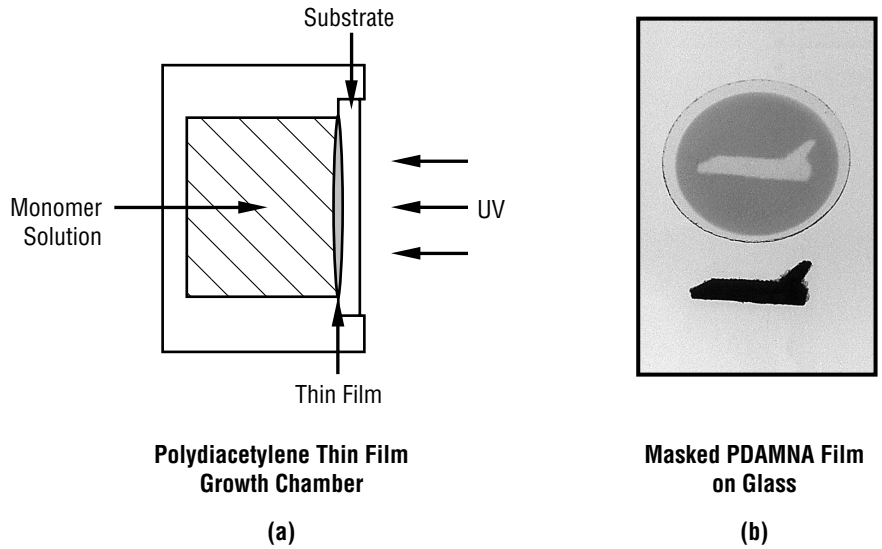

FIGURE 18.—(a) PDA thin film growth chamber, and (b) masked PDAMNA film on glass.

The exact role that the substrate plays in photodeposition of PDA films from solution is not yet fully understood. Apparently, any substrate which is sufficiently transparent to UV light can be used; thus far we have grown PDAMNA films onto glass, quartz, mica, indium-tin oxide-coated glass, polyethylene teraphthalate, KBr, and NaCl. In order to gain some insight into the process that occurs at the surface of the substrate during photodeposition, masking experiments were conducted in which a portion of the substrate is blocked from exposure to the UV light during film deposition. The mask is placed on the *exterior* surface of the substrate (opposite the side on which the film is grown), and thus is not in contact with the solution; it serves merely to protect part of the substrate from the light. Interestingly, the result is that film deposition occurs only where the substrate is directly exposed to the light (see figure above); absolutely no film deposition occurs behind the mask, even though polymerization takes place throughout the bulk solution. This clearly indicates that polymerization is occurring at (or very near) the surface. If this were simply a case of bulk solution polymerization, followed by adsorption of the polymer onto the substrate, the mask, because it is on the outside, should have no effect; film deposition would be expected to occur over the entire substrate.

2. Third-Order NLO Properties of Films

Based on optical microscopy, and on refractive index measurements using waveguide mode analysis, PDAMNA thin films obtained via photodeposition from solution have good optical quality, superior to that of films grown using conventional crystal growth techniques. Considering the simplicity of photodeposition, this technique could make the production of PDA thin films for applications such as NLO devices technologically feasible. Hence the NLO properties of the PDAMNA films were investigated, specifically, their third-order NLO susceptibilities.

Degenerate four-wave mixing experiments carried out at 532 nm on PDAMNA films obtained by photodeposition from solution (thickness around 1.0 μm) yield $\chi^{(3)}$ values on the order of 10^{-8} to

10^{-7} esu. Qualitative measurements indicate that the response time is on the order of picoseconds, which is consistent with an electronic mechanism for the nonlinearity. It should be pointed out that because 532 nm is in the absorption edge of the polymer, the $\chi^{(3)}$ values obtained are resonance-enhanced. Typically, $\chi^{(3)}$ values for PDA's can vary by several orders of magnitude, depending on the degree of resonance enhancement and other factors.[87] The largest reported nonresonant (purely electronic) $\chi^{(3)}$ value for a PDA is on the order of $10^{-9} - 10^{-10}$ esu for PTS single crystals.[103] In order to obtain a valid measure of the inherent nonlinearity of the PDAMNA films, experiments need to be conducted at longer wavelengths where the polymer does not absorb (in the case of PDAMNA, above 700 nm). Preliminary measurements with the PDAMNA films using a Ti-Sapphire laser at 810 nm give $\chi^{(3)}$ values on the order of 10^{-11} esu, with response times on the order of femtoseconds.[104] There are no indications of either one- or two-photon absorption at this wavelength. To ascertain the true potential for device applications (the figures of merit), thorough measurements of light scattering, linear absorption, two- and three-photon absorption, damage thresholds, and so forth must be carried out.[105] Such experiments are underway and will be the subject of future publications.

Thus far, these films have not been studied for second-order NLO properties because they are amorphous; although studies (atomic force microscopy, scanning electron microscopy, and UV-visible spectroscopy) do indicate that there is partial chain alignment in the direction normal to the substrate. At present, the degree of orientation is too low to exploit any potential second-order nonlinearity. However, it may be possible to improve the orientation in the films by means such as electric field poling, surface modification of the substrate, or even modifying the polymer structure (e.g., attaching a liquid crystal moeity). Ordered PDA films would not only be capable of second-order nonlinearity, but should also exhibit increased third-order nonlinearity. Additionally, electronic applications such as one-dimensional conductors require films with aligned polymer chains.

3. Fluid Dynamic Analysis

It is well-known that gravitational effects, such as buoyancy-driven convection, can affect heat and mass transport processes in solution.[106] Photodeposition of PDA films from solution is no exception. We shall first discuss how buoyancy-driven convection can arise during photodeposition of PDAMNA films from solution, and then describe how this convection can affect the morphology, microstructure, and properties of the films obtained. Both the monomer solution and the film generate heat due to absorption of UV radiation. The radiative heating, along with the thermal boundary conditions of the walls of the thin film growth chamber, will give rise to a complex temperature pattern in the solution. Due to the lack of thermodynamic equilibrium, the solution will possess temperature and concentration gradients, and therefore density gradients. These gradients, under the influence of gravity, can induce convective fluid flows in the solution (buoyancy-driven convection).

The onset of thermal convection is determined by a stability parameter known as the Rayleigh number, *Ra*, defined as[106]

$$Ra = \frac{\alpha g d^3 \Delta T}{\nu \kappa} \quad , \tag{4}$$

where α is the coefficient of thermal expansion of the solution; g is the acceleration due to gravity; ΔT is the temperature difference across distance, d, in the solution; ν is the kinematic viscosity; and κ is the thermal diffusivity. For photodeposition of PDAMNA films, the value of ΔT (over a distance of less than 1 mm) can vary from a only a few tenths of a degree to several degrees, depending on the intensity of the UV radiation. In order to grow thicker films (> 1 μ), higher intensity radiation is necessary, making large temperature gradients unavoidable. The intensity and flow pattern of convection can be predicted when the Rayleigh number is known. For instance, for an infinite fluid layer in the horizontal direction with a temperature gradient in the vertical direction (co-linear with gravity), convective motion will occur in the form of rolls with axes aligned horizontal when $Ra > 1{,}708$ (the critical Rayleigh number), while no convection will occur if $Ra < 1{,}708$.[107] The exact value can only be determined by numerical solution of the fluid flow in the chamber. In the case of horizontal temperature gradients (orthogonal to gravity), all values of the Rayleigh number lead to convection, and the magnitude of the velocity of the fluid flow is proportional to the square root of the Rayleigh number.

Density gradients can also arise in the solution due to variations in the concentrations of the chemical species present in the solution. Variations in the monomer concentration are caused by depletion of monomer from the solution at the surface of the growing film and in the bulk. Also generation of dimers, trimers, and other soluble byproducts in the bulk solution may result in additional concentration density gradients. Such solutal gradients, along with the temperature gradients, can give rise to double-diffusive convection. This complicated convective motion is usually analyzed with the aid of the solutal Rayleigh number, in addition to the thermal Rayleigh number.[106] The solutal Rayleigh number, Ra_s, is defined as

$$Ra_s = \frac{\beta g d^3 \Delta C}{\nu D} \quad , \tag{5}$$

where β is the coefficient of concentration expansion; ΔC is the concentration difference across distance, d, in the solution; and D is the diffusion coefficient. Double-diffusive convection flows can be far more complex than simple thermal convection flows.

Hence we see that convection can arise by several means during PDA film photodeposition from solution. The extent of convection, and its intensity and structure, can only be understood through accurate numerical modeling of the fluid motion and thermodynamic state of the system.

4. Transport of Particles from Bulk Solution

One significant effect of convection can be seen when PDAMNA films grown in 1-g are viewed under an optical microscope: they exhibit small particles of solid polymer embedded throughout. These form when polymer chains in the bulk solution collide due to convection and coalesce into small solid particles, on the order of a few hundedths of a micron in size. Because these particles are so small, almost colloidal in nature, they do not sediment out readily, and thus remain suspended in the bulk solution. Convection then transports these particles to the surface of the growing film where they become embedded. These particles are defects that can scatter light and thus lower the optical quality of the films.

To study the effects of convection on the occurrence of these particles in the films, the growth chamber was placed in different orientations with respect to gravity in order to vary the fluid flow pattern.[108] PDAMNA films were grown with the chamber vertical (irradiating from the top) and with the chamber horizontal (irradiating from the side). In the case when the chamber is vertical and the solution is irradiated from the top, the axial temperature gradient is vertical with respect to gravity, and the bulk solution is stably stratified because warmer, less dense solution is above cooler, more dense solution. Thus in this orientation, convection should be minimized. In the case when the chamber is horizontal and the solution is irradiated from the side, the axial temperature gradient is horizontal with respect to gravity, which makes the density gradients less stable. Hence convection should be much more pronounced in this orientation. Numerical simulations of the fluid flow are consistent with these expectations.[108]

This is reflected in the distribution of solid particles observed in the PDAMNA films grown in the two different orientations. Films grown with the chamber horizontal clearly contain a greater concentration of particles than films grown with the chamber vertical (fig. 19). This is consistent with expectations based on the relative amounts of convection in the two orientations; films grown under increased convection contain more particles than those grown under less convection. Also, waveguiding experiments with these films demonstrate that the films containing more particles exhibit greater light scattering than those containing fewer particles.

Note that even the film grown in the vertical orientation, where convection is minimized, still contains particles. Thus while convection is lessened, in this case, it is not eliminated. There are two reasons for this. First, there are still radial thermal density gradients in the horizontal direction even when the chamber is vertical because the solution near the side walls is cooler than that near the center; these can give rise to convection. Also, because the substrate is transparent to UV light, it is not heated directly by the radiation; the only means by which it receives heat is via conduction. Thus, initially, there will be some heat flow from the warm solution to the cooler substrate, producing a very shallow unstable thermal density gradient in the immediate vicinity of the substrate/solution interface, which sits above the stably stratified bulk solution. Any convection initiated in this unstable layer may penetrate deeper into the stable layer below, giving rise to the phenomenon of penetrative convection.[109] The bottom line is that even under optimum conditions in 1-g, convection is still present during PDA thin film photodeposition from solution, causing particles in the films.

Not only can convection affect the transport of particles which are polymerized from the bulk solution, it can also transport colloidal particles which are purposely introduced into the system to alter the optical properties. The study of the effect of composite geometries on the NLO properties of materials is an active area of research. One of the most commonly studied systems, discussed earlier, involves small metal inclusion particles surrounded by a continuous host medium. The linear optical properties of these composites are described by the theory of Maxwell Garnett.[110] In recent years the model has been extended to include nonlinear materials.[111 112] Unfortunately, assimilation of metal particles into highly nonlinear solid-state materials is difficult using traditional chemical techniques because most highly nonlinear polymeric host candidates require organic solvents which are ncompatible with the colloid. Ion implantation is a realistic alternative but is not readily available

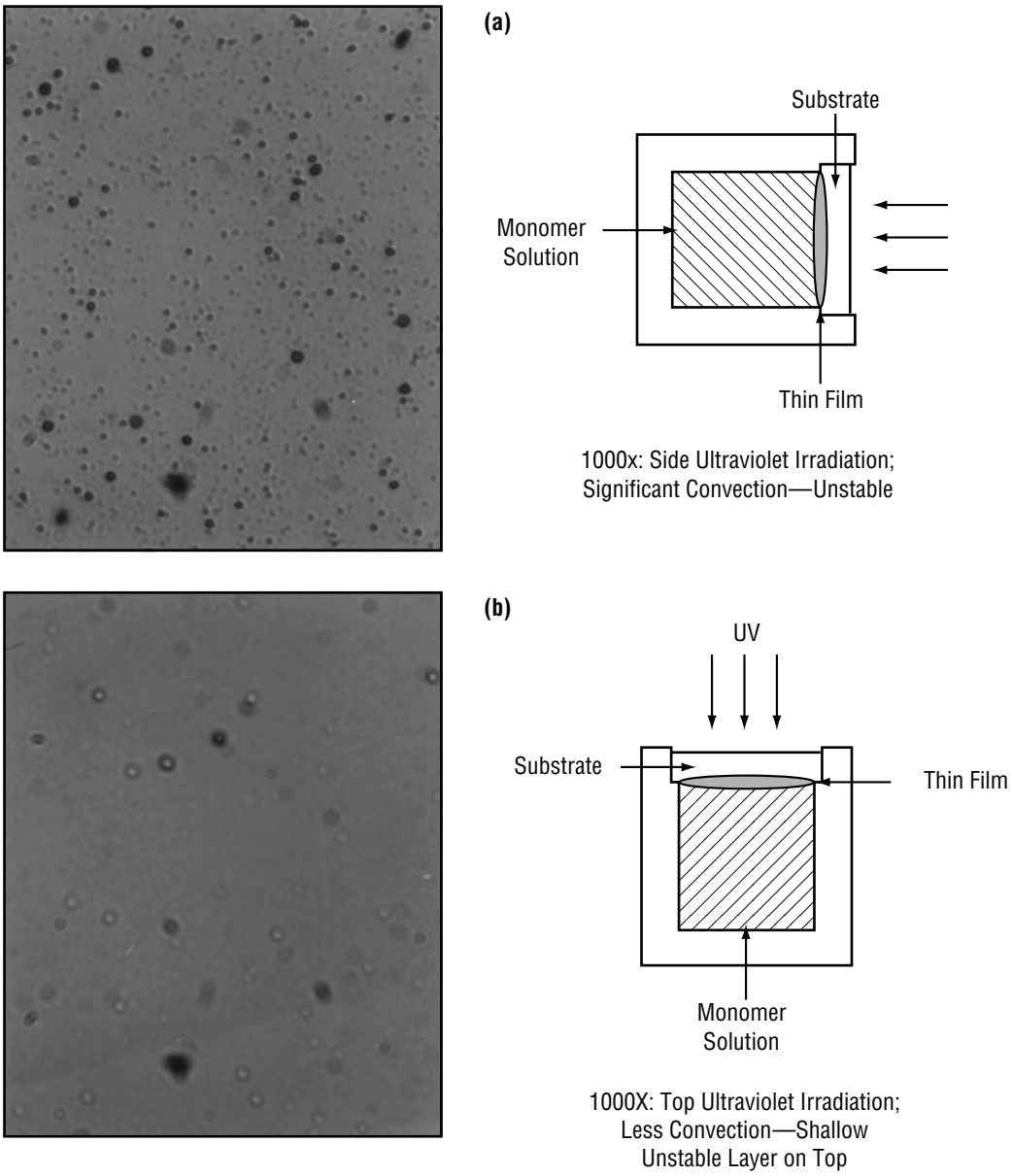

FIGURE 19.—PDAMNA films grown in two different orientations: (a) films grown with the chamber horizontal, and (b) films grown with the chamber vertical.

in most laboratories. Moreover, the distribution of metal in the axial direction follows a Gaussian profile. Recently, however, Brust et al.[113] functionalized gold particles with thiol groups which serve to protect the particles from solvent degradation and attack. Interestingly, the colloidal metal can actually be dried and stored without agglomeration. The thiol groups in this case have little effect on the optical properties of the colloid. These thiol-capped metal particles can then be resuspended in many organic solvents and incorporated into the PDAMNA films through photopolymerization. Hence, this recipe offers a simple way to introduce small metal particles into highly nonlinear polymers. The resulting films, however, suffer from gradients in the metal concentration which are clearly visible under

reflected room light. Moreover, the films have a much higher concentration of metal than would be expected from a diffusional process. Hence, these gradients most likely arise from the process of convection. Convection often tends to destroy the homogeneity of particle-doped systems, whether it be colloidal metal films or doped porous glass. In this case, the metal particle dopants serve not only to modify the NLO properties of the system, but also to elucidate the role of convection in the formation of polymeric thin films.

5. Effects of Convection on Kinetics, Morphology, and Microstructure

We have discussed how convection can transport particles of solid polymer precipitated from the bulk solution into the films. However, convection can also affect film deposition at the molecular level. To gain some insight into these effects, it is necessary to understand the kinetics of film deposition.

The rate of PDA film photodeposition from solution can be given by the expression[114]

$$\frac{dl}{dt} = k\, I^m\, C^n \quad , \tag{6}$$

where l is film thickness, t is time, I is the intensity of the UV radiation, C is monomer concentration, m and n are the orders of the reaction in radiation intensity and monomer concentration, respectively, and k is the rate constant. Initial results indicate that for photodeposition (using 365 nm wavelength light) of PDAMNA films from 1,2-dichloroethane at ambient temperature (25 °C), $m = 1.0$, $n = 0.5$, and $k = 3.2\times10^{-7}$ (mks units).[114]

Additionally, it can be shown from the principles of chemical kinetics (Arrhenius equation)[115] that the rate constant (k) is given by

$$k = A e^{-E/k_b T} \quad , \tag{7}$$

where E is the activation energy of the reaction, k_b is Boltzman's constant, T is temperature, and A is a preexponential factor related to the frequency of collisions of molecules with the surface of the growing film.

The equations above clearly show how the rate of PDA film photodeposition from solution depends on variables such as temperature and monomer concentration. The effects of convection can also be gleaned from these equations. We know that convection affects heat and mass transport to and from the surface of the growing film, which is reflected in the temperature and concentration profiles along the surface. Variations in these parameters along the surface of the film, in accordance with the above equations, will cause variations in the rate of film deposition, leading to uneven film growth. This will be especially pronounced if the fluid flow along the surface varies drastically, or is turbulent. Thus we see how convection can directly affect the kinetics of PDA film photodeposition from solution, and thereby affect the morphology (thickness and surface roughness) of the films.

Finally, convection may also play a role in affecting the microstructure of the films; specifically, the molecular orientation of the PDA chains. Preliminary studies conducted using atomic force microscopy and x-ray photoelectron spectroscopy indicate that films photodeposited onto quartz (in 1-g) for very short duration of time (a few minutes) exhibit good polymer chain alignment in the direction normal to the substrate, while films grown for longer duration show significantly poorer chain alignment. Thus in the early stages of deposition there appears to be some tendency for orientation, which lessens as the reaction proceeds and the polymer chains grow. This could be due to the fact that as the film grows, any influence that the substrate may have on molecular orientation at the film surface decreases. However, in this case the substrate is amorphous quartz; hence, ordering of the polymer chains by the substrate (i.e., epitaxy) is not expected. Therefore another possibility for the decrease in order is convection. The turbulent and chaotic molecular motions that occur during convection may cause the chains to become entangled and matted around each other as they grow longer. Also, variations in temperature and monomer concentration along the film surface, influenced by convection, can affect molecular orientation, and possibly even polymer chain packing densities. Discerning the role that convection plays in affecting molecular orientation is an essential part of any fundamental study.

6. Growth of Films in Microgravity

An experiment was recently conducted aboard the Space Shuttle *Endeavour* (CONCAP–IV) in which photodeposition of PDAMNA films from solution was carried out in microgravity.[108] In this environment buoyancy-driven convection can essentially be eliminated. Because of unplanned orbiter maneuvers during the mission, leading to extraneous accelerations, and limitations of the flight hardware, results varied somewhat among samples. However, the best space-grown film clearly exhibits fewer particles than the best ground-based films (fig. 20). These few particles may have resulted from slight mixing in the solution caused by the orbiter motions, or possibly, they may have nucleated on the surface the film itself. Nonetheless, the initial results are very encouraging; it appears that the lack of convection can indeed lead to PDAMNA films with significantly fewer defects, and thus greater optical quality. Further characterizations of the space-grown films are currently underway.

This study clearly shows that photodeposition of PDA thin films in unit gravity occurs in highly convective environments, and that this convection can influence the morphology and quality of the films. Indeed, even when irradiation occurs from the top of the cell, the most stable stratified cell orientation, defects remain in the films due to the persistence of buoyancy-driven convection. To achieve homogeneity, minimal scattering centers, and possible molecular order, photodeposition of polymer films by UV light exposure must proceed in a microgravity environment. Fluid mechanics simulations are useful for establishing gravitational sensitivity to this recently discovered process[45] for preparing thin films having quite promising NLO characteristics.

B. Polymer Thin Films by Electrochemical Polymerization

Electrochemical polymerization is a method that should be thoroughly investigated for use in fabricating thin film waveguides. The procedure is relatively straightforward and films can be fabricated using many commercially available materials. Another desirable feature is that NLO films might be

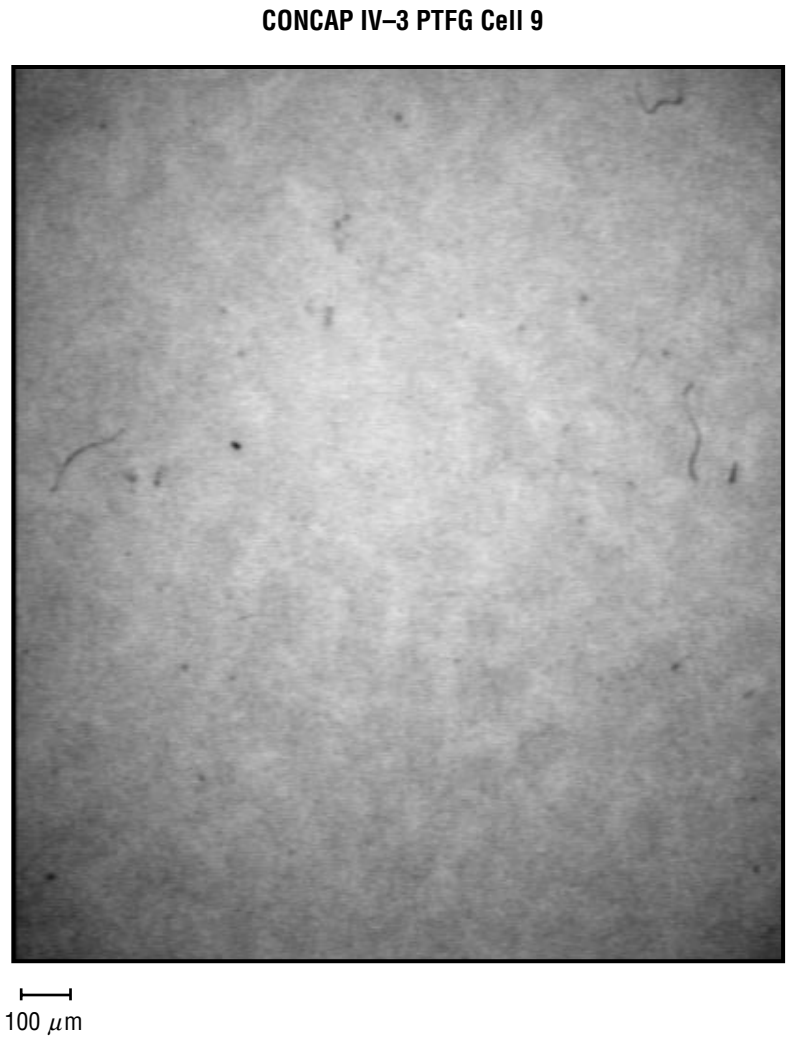

FIGURE 20.—PDAMNA films grown in space. The best space-grown films clearly exhibit fewer particles than the best ground-based films.

prepared on the surface of various substrates during polymerization for the fabrication of devices. In addition, this method has been used to synthesize several polymers that include pT's, polazulene, and polypyrrole.

Polythiophenes are promising materials for NLO applications because of their large third-order optical nonlinearities, environmental stability, and structural versatility. Their potential suitability for devices was demonstrated by Dorsinville et al.[116] who measured the NLO properties of thin films of pT, polythieno(3,2-b), thiophene (pTT), polydithieno(3,2-b,2',3'-d)thiophene (pDTT). The $\chi^{(3)}$ values at 532 nm for pT, pTT, and pDTT were 6.6×10^{-9} esu, 5.9×10^{-9} esu, and 11.3×10^{-9} esu, respectively. Electropolymerization of the monomers was performed in a two-compartment cell with indium-tin oxide electrodes. Typical thickness of films were 0.5–2 μm. In addition, Logsdon et al.[117] obtained a $\chi^{(3)}$ value of 10^{-9} esu for LB films of poly(3-dodecylthiophene). The polymer was first prepared by

electrochemical polymerization. This was then used to prepare LB films. The electrochemical process was carried out at 5 °C using nitrobenzene as the solvent, tetra-n-butylammonium hexaflurophosphate as the electrolyte, indium-tin oxide as the cathode, and a platinum coil as the cathode.

The prospect for using microgravity processing to produce better polymer films by electrochemical reactions or learn principles that might be used to improve processing on Earth should be explored since there is evidence that electrodeposition of metals in low-g results in deposits that have significant differences relative to those prepared on Earth. Erhard[118 119] found that nickel deposited at high rates in microgravity during a suborbital rocket flight produced an amorphous or nanocrystalline film with grains so small that x-ray diffraction peaks associated with the crystalline structures were not seen. Further studies involving the electrodeposition of metals in microgravity have been performed by Riley and coworkers.[120–122]

IV. PROTOTYPE DEVICES BASED ON SECOND- AND THIRD-ORDER NLO ORGANICS AND POLYMERS

A. Electro-Optic Polymer Advances

It is an accepted conclusion that the development of all-optical devices will be gradual and will include hybrid devices in which electrons interface with photons. The advent of electro-optics occurred several years ago when researchers realized that photons could respond to electrons through certain media such as lithium niobate ($LiNbO_3$). This route towards the development of all-optical devices demands immediate and intensive searches for the ideal hybrid, which requires appropriate processing techniques and large second-order characteristics in the materials of interest. It is this technology requirement that enhances the criticality of asymmetry in crystal packing and heightens the potential value of microgravity processing. The goal is to exploit maximum and optimal directionality of hyperpolarizabilities in inorganic or organic crystals interacting with electric fields, and their capacity to modulate light. Alignment of polymers and macromolecules to take advantage of predicted second-order superiority in many of these molecules could provide the desired effects.

There have been several significant advances in the development of electro-optic devices based on polymers. One of the problems associated with organic systems is the inherent “brittle” nature of pure materials as a result of weak Van der Waals intermolecular interactions in contrast to strong ionic and covalent bonds characteristic of inorganics. Dalton et al.[123] has addressed this problem by preparing a variety of highly cross-linked polymers based on spin-casting and poling a polymethacrylate with “dangling chromophores.” The resultant cross-linked polymer films are “hard” and exhibit very high electro-optic coefficients. These materials retain their optical nonlinearity for several thousand hours at relatively high temperatures (90–150 °C). Optoelectronic modulators developed by this group based on these and other materials and processes are available as prototypes and are capable of efficiently converting electronic signals into optical signals. These researchers and some others in the field believe that polymer-based modulators will outperform conventional inorganic devices and should be significantly less expensive to prepare.

Marder and coworkers[124] have played a key role in these developments, including the development of a heterocyclic molecule with a strong electron donor and strong acceptors. This molecule is highly soluble in a polycarbonate matrix which, after poling, yields a material with very high second-order coefficients and good mechanical strength. Although this material does not have good thermal stability, the contribution is a significant one toward the search for the ideal electro-optic material based on organic and polymeric materials.

B. All-Optical Switching

A Mach-Zehnder interferometer (fig. 21a) is an example of an on-off switch. Switching occurs when the phase of one arm is shifted by π relative to the phase of the other arm. For all-optical switching, the phase shift may be achieved by introducing an NLO material into one of the arms of the interferometer or by using a nonlinear material for the entire interferometer and making one arm longer than the other—an asymmetric Mach-Zehnder interferometer. For fused silica fibers, long lengths of fiber are required to reduce the switching energy due to the weak nonlinearity, and this makes it difficult to maintain the stability of the interferometer. Thus, for fibers, a very ubiquitous approach is to use an NLO loop mirror (fig. 21b). The loop mirror is very stable since it is a common path interferometer.

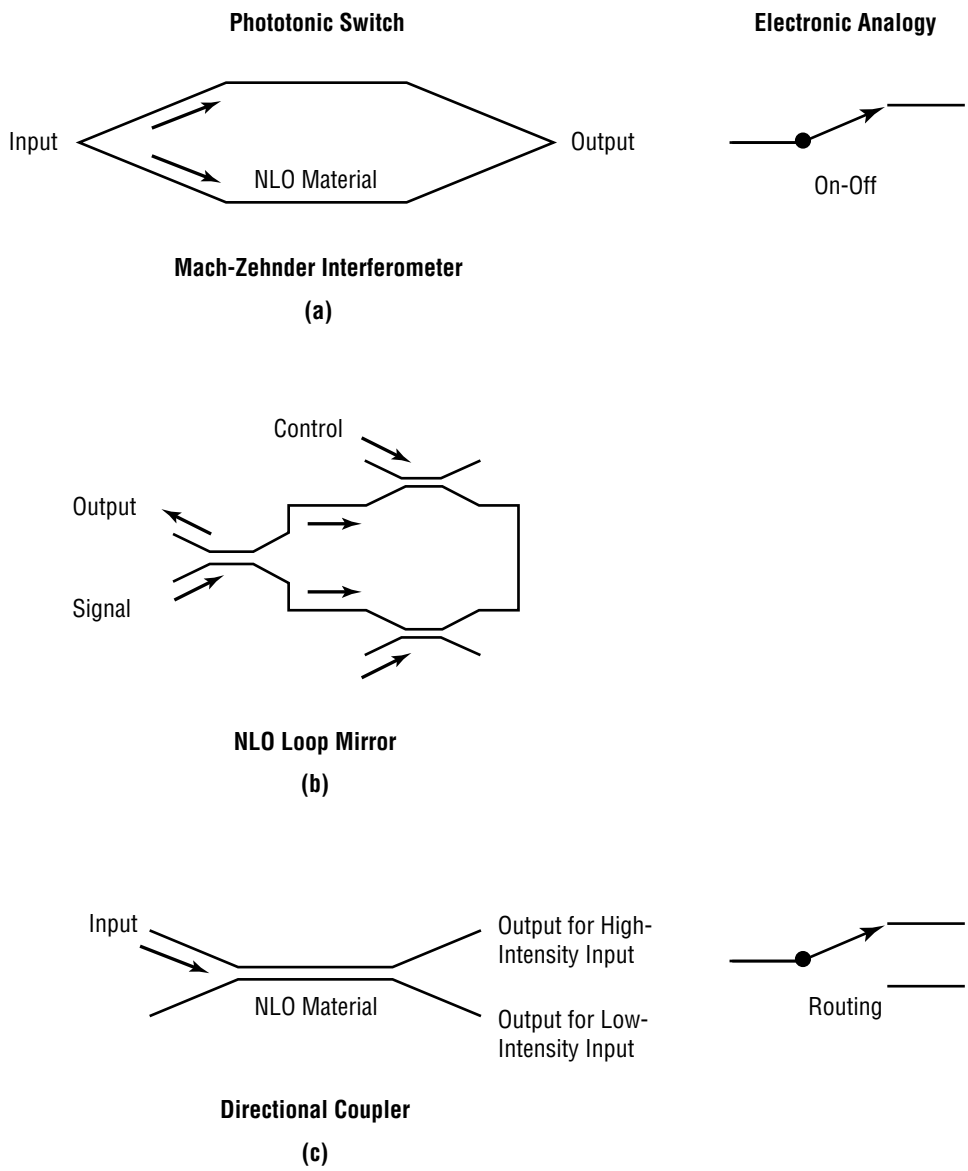

FIGURE 21.—(a) Mach-Zehnder interferometer, (b) NLO loop mirror, and (c) nonlinear directional coupler and their electronic analogs.

The required phase shift is achieved through cross-phase modulation of the signal by an orthogonal polarized control pulse. Since the control pulse propagates in one direction, the index change occurs only for the copropagating signal pulse. The bottom coupler extracts the control pulse from the loop.

Although NLO loop mirrors provide a variety of controls and options for the user, more compact devices are required for integrated optics applications and these require materials with higher nonlinearities to keep the switching energy low enough to be practically useful. The NLDC described earlier (fig. 21c) or the Mach-Zehnder interferometer are better suited for these applications. Efficient femtosecond all-optical switching has been demonstrated in GaAlAs passive semiconductor systems at energies below half the band gap in a number of different devices.[125–128] Although TPA is no longer a problem for energies below half the band gap, three-photon absorption can still impede device performance.[129] To avoid three-photon absorption, Stegeman et al. employed a longer interaction length in an NLDC to reduce the switching power, thus avoiding higher order nonlinear absorption.[130] A switching energy of 65 pJ was achieved. GVD had little affect for 6.6-ps pulses but severely affected device operation for 430-fs pulses. An important trait of these semiconductor systems is that by varying the alloy composition, the half-bandgap energy can be tuned anywhere within the telecommunications window of 1.3–1.6 μm. An alternative approach to working below half-bandgap is to utilize the large, fast nonlinearity at the transparency point of an active semiconductor. Lee et al. have reported subpicosecond 10-pJ switching at 880 nm in a current injected GaAs/AlGaAs multiple-quantum-well NLDC.[131]

Organic materials such as conjugated polymers, although less developed than semiconductor systems, are highly promising because they have generally larger nonlinearities, are more facile for molecular tailoring, and more malleable than their inorganic counterparts. Many conjugated polymers are difficult to pattern into waveguides, however, and it was nearly a decade before switching in an NLDC made from a soluble PDA commonly known as poly(4-BCMU) (poly-[5,7-dodecadiyne-1,1,12-diolbis(n-butoxycarbonylmethylurethane)]) was assessed by Townsend et al.[132] An interesting fabrication technique was utilized in which the substrate was first patterned with high index ion-exchanged channels before spin-coating. The underlying channel provides lateral optical confinement, requiring no patterning of the polymer itself. Since, however, the refractive index of the polymer is higher than that of the channels, the polymer contains the majority of the field and hence provides the necessary NLO interactions. Although a slower thermo-optical switching was attained, incomplete ultrafast switching at 1.06 μm was observed due to TPA. Irreversible photoinduced bleaching has also been shown to produce index changes in poly(4-BCMU) that are large enough to fabricate channel waveguides.[133] Thakur et al. have demonstrated all-optical phase modulation in a PDA by using a photolithographic technique to fabricate channel waveguides in single crystal films of PTS prepared by a shear method.[103] The figures of merit for PTS at the communications wavelengths of 1.3 and 1.55 μm have been measured by Kim et al. and indicate its promise for all-optical switching applications.[134] More recently, it has been demonstrated that there exists a class of diacetylenes that form this transparent amorphous polymer films reading from monomer solutions irradiated with long wavelength ultraviolet light through a quartz or glass window, which also serves as the substate.[45 46] As described earlier, this process may be exploited to produce integrated optical structures in PDA.

With only marginal improvements expected in the GaAs/AlGaAs passive semiconductors expected in the near future, attention has turned to the polymeric systems. Although the technology of fabricating third-order polymeric integrated optics is still maturing, the figures of merit are very promising. We believe that, because of the uniqueness of polymeric materials, simpler and less costly techniques such as those presented here can develop, eventually complementing standard lithographic techniques.

REFERENCES

1. Nayar, B.K,; and Winter, C.S.: *Optical and Quantum Electronics*, vol. 22, p. 297, 1990.

2. Carter, G.M.; Chen, Y.J.; and Tripathy, S.K.: *Appl. Phys. Lett.*, vol. 43, p. 891, 1988.

3. Kajzar, F.; Meissier, J.; Zyss, J.; and Ledoux, I.: *Opt. Commun.*, vol. 45, p. 133, 1983.

4. Kajzar, F.; and Messler, J.: *Thin Solid Films*, vol. 11, p. 132, 1988.

5. Debe, M.K.; and Kam, K.K.: *Thin Solid Films*, vol. 186, p. 289, 1990.

6. Frazier, D.O.; Penn, B.G.; Witherow, W.K.; and Paley, M.S.: *SPIE Crystal Growth in Space and Related Diagnostics*, vol. 1557, p. 86, 1991.

7. Wegner, G.Z.: *Naturforsch*, vol. 246, p. 824, 1969.

8. Thakur, M.; and Meyler, S.: *Macromolecules*, vol. 18, p. 2341, 1985.

9. Thakur, M.; Carter, G.M.; Meyler, S.; and Hryniewicz, H.: *Polymer Preprints*, vol. 27(1), p. 49, 1986.

10. Ledoux, I.; Josse, D.; Vidakovic, P.; and Zyss, J.: *Optical Engineering*, vol. 27(1), p. 49, 1986.

11. Islam, M.N.: *Phys. Today*, p. 34, May 1994.

12. Franken, P.A.; Hill, A.E.; Peters, C.W.; and Weinreich, G.: *Phys. Rev. Lett.*, vol. 7, p. 118, 1961.

13. Davydov, B.L.; Derkacheva, L.D.; Dunina, V.V.; Zhabotinskii, M.E.; Zolin, V.F.; Koreneva, L.G.; and Samokhina, M.A.: *Opt. Spectrosc.*, vol. 30, p. 274, 1971.

14. Marcy, H.O.; Rosker, M.J.; Warren, L.F.; Cunningham, P.H.; Thomas, C.A.; Deloach, L.A.; Velsko, S.P.; Ebbers, C.A.; Liao, J.H.; and Kanatzidis, M.G.: *Opt. Lett.*, vol. 20, p. 252, 1995.

15. Rosenberger, F.; Howard, S.B.; Sowers, J.W.; and Nyce, T.A.: *J. Crystal Growth*, vol. 129, p. 1, 1993.

16. Pusey, M.; Witherow, W.; and Naumann, R.: *J. Crystal Growth*, vol. 90, p. 105, 1988.

17. Pusey, M.: Fourth International Conference on Crystallization of Biological Macromolecules, Freiburg, Germany, August 18–23, 1991.

18. Agrawal, G.P.: *Nonlinear Fiber Opt.*, Pub.: Academic Press, San Diego, CA, 1995.

19. Jensen, S.M.: *IEEE J. Quant. Elect.*, QE–18, p. 1580, 1982.

20. Mizrahi, V.K.; Delong, K.W.; Stegeman, G.I.; Saifi, M.A.; Andrejco, M.J.: *Opt. Lett.*, vol. 14, p. 1140, 1989.

21. Sheik-Bahae, M.; Hagan, D.J.; and Van Stryland, E.W.: *Phys. Rev. Lett.*, vol. 65, p. 96, 1990.

22. Delong, W.K.; and Stegeman, G.I.: *Appl. Phys. Lett.*, vol. 57, p. 2063, 1990.

23. Hache, F.; Ricard, D.; Flytzanis, C.; and Kreibig, U.: *Appl. Phys. A*, vol. 47, p. 47, 1988.

24. Lehoczky, S.L.; Szofran, F.R.; Gillies, D.C.; Cobb, S.D.; Su, C.H.; Sha, Y.G.; and Andrews, R.N.: NASA Conference Publication, vol. 3272 I, 1994.

25. Smith, D.D.: *Ph.D. Thesis*, University of Alabama in Huntsville, Huntsville, AL, 1996.

26. Turkevich, J.; Stevenson, P.C.; and Hillier, J.: The Size and Shape Factor in Colloidal Systems, A General Discussion of the Faraday Society, vol. 11, p. 55, 1951.

27. Fröhlich, H.: *Theory of Dielectrics*, Pub.: Oxford University Press, London, 1958.

28. Swatton, S.N.R.; Welford, K.R.; Till, S.J.; and Sambles, J.R.: *Appl. Phys. Lett.*, vol. 66, p. 1868, 1995.

29. Stegeman, G.I.; and Miller, A.: in *Photonics and Switching*, Eds.: J.E.Midwinter, Academic Press, London, p. 81-145, 1994.

30. Delong, K.W.; Rochford, K.B.; and Stegeman, G.I.: *Appl. Phys. Lett.*, vol. 55, p. 1823, 1989.

31. Yang, A.V.; Stegeman, G.I.; and Aitchison, J.S.: *Opt. Lett.*, vol. 17, p. 710, 1992.

32. Asobe, M.; Naganuma, K.; Kaino, T.; Kanamori, T.; Tomaru, S.; and Kurihara, T.: *Appl. Phys. Lett.*, vol. 64(22), p. 2922, 1994.

33. Paley, M.S.; Frazier, D.O.; McManus, S.P.; Zutaut, S.E.; and Sangahadasa, M.: *Chem. Mater.*, vol. 5, p. 1641, 1993.

34. Debe, M.K.: *Prog. Surf. Sci.*, vol. 24(1-4), 1, 1987.

35. Liu, C.J.; Debe, M.K.; Leung, P.C.; and Francis, C.V.: *Appl. Phys. Comm.*, vol. 11(2–3), p. 151, 1992.

36. Kam, K.K.; Debe, M.K.; Poirier, R.J.; and Drube, A.R.: *J. Vac. Sci. Technol.*, vol. A5(4), p. 1914, 1987.

37. Debe, M.K.; Kam, K.K.; Liu, C.J.; and Poirier, R.J., *J. Vac. Sci. Technol.*, vol. A6, p. 1907, 1988.

38. Debe, M.K.: *J. Appl. Phys.*, vol. 55, p. 3354, 1984; Debe, M.K., and Tommet, T.N.: *J. Appl. Phys.*, vol. 62, p. 1546, 1987.

39. Debe, M.K.; Poirier, R.J.; and Kam, K.K.: *Thin Solid Films*, vol. 197, p. 335, 1991.

40. Debe, M.K.; and Field, D.R.: *J. Vac. Sci. Technol.*, vol. A9, p. 1265, 1991.

41. Debe, M.K.: *J. Vac. Sci. Technol.*, vol. A10(4), p. 2816, 1992.

42. Debe, M.K.: *J. Vac. Sci. Technol.*, vol. 21, p. 74, 1992.

43. Debe, M.K.; Poirier, R.J.; Erickson, D.D.; Tommet, T.N.; Field, D.R.; and White, K.M.: *Thin Solid Films*, vol. 186, p. 257, 1990.

44. Debe, M.K.; and Poirier, R.J.: *Thin Solid Films*, vol. 186, p. 327, 1990.

45. Paley, M.S.; Frazier, D.O.; McManus, S.P.; Donovan, D.N.: U.S. Patent No. 5,451,433, September 19, 1995.

46. Paley, M.S.; Frazier, D.O.; Abdeldeyem, H.A.; Armstrong, S.; and McManus, S.P.: *J. Am. Chem. Soc.*, vol. 117(17), p. 4775, 1995.

47. Pearson, E.; Witherow, W.K.; and Penn, B.G.: private communication.

48. Hotta, S.; Hosaka, T.; Soga, M.; and Shimotsuma, W.: *Syn. Met.*, vol. 9, p. 381, 1984.

49. Tanaka, S.; Sato, M.; and Kaeriyama, K.: *Makromol. Chem.*, p. 1295, 1984.

50. Waltman, R.J.; and Bargon, J.: *Can. J. Chem.*, vol. 64, p. 76, 1986.

51. Yang, L.; Dorsinville, R.; Wang, Q.Z.; Zou, W.K.; Ho, P.P.; Yang, N.L.; Alfano, R.R.; Zamboni, R.; Danieli, R.; Ruani, G.; and Taliani, C.: *J. Opt. Soc. Am.*, vol. 6(B), p. 753, 1989.

52. Dorsinville, R.; Yang, L.; Alfano, R.R.; Zamboni, R.; Danieli, R.; Ruani, G.; and Taliani, C.: *Opt. Lett.*, vol. 14(23), p. 1321, 1989.

53. Abi-Akar, H.M.: Ph.D. Thesis, University of Alabama in Huntsville, Huntsville, AL, 1992.

54. Abi-Akar, H.; Riley, C.; Coble, H.D.; and Maybee, G.: *J. Mat. Sci.*, to be published.

55. Ho, Z.Z.; Ju, C.Y.; and Hetherington, W.M., III: *J. Appl. Phys.*, vol. 62, p. 716, 1987.

56. Shirk, J.S.; Lindle, J.R.; Bartoli, F.J.; Hoffman, C.A.; Kafafi, Z.H.; and Snow, A.W.: *Appl. Phys. Lett.*, vol. 55, p. 1287, 1989.

57. Wu, J.W.; Heflin, J.R.; Norwood, R.A.; Wong, K.Y.; Zamani-Khamiri, O.; Garito, A.F.; Kalyanaraman, P.; and Sounik, J.: *J. Opt. Soc. Am.*, B, vol. 6(4), p. 707, 1989.

58. Matsuda, M.; Okada, S.; Masaki, A.; Nakanishi, H.; Suda, Y.; Shigehara, K.; and Yamada, Y.: *Proc. SPIE*, vol. 1337, p. 105, 1990.

59. Hosoda, M.; Wada, T.; Yamada, A.; Garito, A.F.; and Sasabe, H.: *Jpn. J. Appl. Phys.*, vol. 30, p. L1486, 1991.

60. Hoshi, H.; Nakamura, N.; and Maruyama, Y.: *J. Appl. Phys.*, vol. 70, p. 7244, 1991.

61. Suda, Y.; Shiegehara, K.; Yamada, A.; Matsuda, H.; Okada, S.; Masaki, A.; and Nakanishi, H.: *SPIE*, vol. 1560, p. 75, 1991.

62. Casstevens, M.K.; Samoc, M.; Pfleger, J.; and Prasad, P.N.: *J. Chem. Phys.*, vol. 92, p. 2019, 1990.

63. Prasad, P.N.; and Williams, D.J.: Introduction to Nonlinear Optical Effects in Molecules and Polymers, Pub.: Wiley Interscience, NY, p. 205, 1991.

64. Reeves, R.J.; Powell, R.C.; Chang, Y.H.; Ford, W.T.; and Zhu, W.: *Opt. Mater.*, vol. 5, p. 43, 1996.

65. Ho, Z.Z.; and Peyghambarian, N.: *Chem. Phys. Lett.*, vol. 148, p. 107, 1988.

66. Williams, V.S.; Mazumdar, S.; Armstrong, N.R.; Ho, Z.Z.; and Peyghambarian, N.: *J. Phys. Chem.*, vol. 96, p. 4500, 1992.

67. Wada, T.; Matsuoka, Y.; Shigehara, K.; Yamada, A.; Garito, A.F.; and Sasabe, H.: *Mater. Res. Soc. Symp. Proc.*, vol. 12, p. 75, 1989.

68. Shirk, J.S.; Lindle, J.R.; Bartoli, F.J.; Hafafi, Z.H.; Snow, A.W.; and Boyle, M.E.: *Int. J. Nonlinear Opt. Phys.*, vol. 1, p. 699, 1992.

69. Sastre, A.; Torres, T.; Diaz-Garcia, M.A.; Aguillo-Lopez, F.; Dhenqaut, C.; Brasselet, S.; Ledoux, I.; and Zyss, J.: *J. Am. Chem. Soc.*, vol. 118, p. 2746, 1996.

70. Suslick, K.S.; Chen, C.; Meredith, G.R.; and Cheng, L.: *J. Am. Chem. Soc.*, vol. 114, p. 6928, 1992.

71. Li, D.; Swanson, B.I.; Robinson, J.M.; Hoffbarrer, M.A.; *J. Am. Chem. Soc.*, vol. 115, p. 6975, 1993.

72. Wada, T.; Yamanda, S.; Matsuoka, Y.; Grossmn, C.H.; Shigehara, K.; Sasbe, H.; Yamada, A.; and Garito, A.F.: in *Nonlinear Optics of Organics and Semiconductors*, Pub.: T.Kobayashi, Springer Berlin, p. 292, 1989.

73. Hosada, M.; Wada, T.; Yamada, A.; Garito, A.; and Sasabe, H.: Jpn. J. Appl. Phys., vol. 30(8B), p. L1486, 1991.

74. Chollet, P.A.; Kajzar, F.; and LeMoigne, J.: *SPIE*, vol. 1273, p. 87, 1990.

75. Kumagai, K.; Mitzutani, G.; Tsukioka, H.; Yamauchi, T.; and Ushioda, S.: *Phys. Rev. B*, vol. 48(19), p. 14488, 1993.

76. Yamada, T.; Hoshi, H.; Ishikawa, K.; Takezoe, H.; and Fukuda, A.: *Jpn. J. Appl. Phys.*, vol. 34, p. L299, 1995.

77. Debe, M.K.; and Kam, K.K.: *Thin Solid Films*, vol. 186, p. 289, 1990.

78. Debe, M.K.; and Poirier, R.J.: *Thin Solid Films*, vol. 186, p. 327, 1990.

79. Debe, M.K.: *J. Vc. Sci. Technol.*, vol. A4(3), p. 273, 1986.

80. Debe, M.K.: *J. Appl. Phys.*, vol. 55(9), p. 3354, 1984; Debe, M.K.; and Tommet, T.N.: *J. Appl. Phys.*, vol. 62, p. 1546, 1987 erratum.

81. Abdeldayem, H.; Frazier, D.O.; Penn, B.G.; Witherow, W.K.; Banks, C.; Smith, D.D.; and Sunkara, H.: *Opt. Comm.*, submitted, 1996.

82. Casstevens, M.K.; Samoc, M.; Pfleger, J.; and Prasad, N.P.: *J. Chem. Phys.*, vol. 92(3), p. 2019, 1990.

83. See, for example, A.Yariv: *Quantum Electronics*, 2nd Ed., Wiley, NY, 1975.

84. Hercher, M.: *Appl. Opt.*, vol. 6(5), p. 947, 1967.

85. Bloor, D.; and Chance, R.R., Eds.: *Polydiacetylenes*, Pub.: Martinus Nijhoff, Dordrecht, The Netherlands, 1985.

86. Chemla, D.S.; and Zyss, J., Eds.: *Nonlinear Optical Properties of Organic Molecules and Crystals,* Vol. *2*, Pub.: Academic Press, Orlando, FL, 1987.

87. Prasad, P.N.; and Williams, D.J.: *Introduction to Nonlinear Optical Effects in Molecules and Polymers,* Pub., John Wiley and Sons, Inc.: NY, 1991; ibid, 232.

88. Carter, G.M.; Thakur, M.K.; Chen, Y.J.; and Hryniewicz, J.V.: *Appl. Phys. Lett.*, vol. 47, p. 457, 1985.

89. Hermann, J.P.; and Smith, P.W.: Digest of Technical Papers—11th International Quantum Electronics Conference, p. 656, 1980.

90. Paley, M.S.; Frazier, D.O.; Abdeldeyem, H.A.; and McManus, S.P.: *Chem. Mater.*, vol. 6(12), p. 2213, 1994.

91. Tsiboulkis, J.; Werninck, A.R.; Shand, A.J.; and Milburn, G.H.W.: *Liquid Crystals*, vol. 3(10), p. 1393, 1988.

92. Kim, T.; Crooks, R.M.; Tsen, M.; and Sun, L.: *J. Am. Chem. Soc.*, vol. 117, p. 3963, 1995.

93. Cheong, D.W.; Kim, W.H.; Samuelson, L.A.; Kumar, J; and Tripathy, S.K.: *Macromolecules*, vol. 29, p. 1416, 1996.

94. Kim, W.H.; Bihari, B.; Moody, R.; Kodali, N.B.; Kumar, J.; and Tripathy, S.K.: *Macromolecules*, vol. 28, p. 642, 1995.

95. Sandman, D.J., Ed.: *Solid State Polymerization*, Pub.: American Chemical Society, Washington, DC, 1987.

96. Frazier, D.O.; Hung, R.J.; Paley, M.S.; Penn, B.G.; and Long, Y.T.: *J. Crys. Growth*, vol. 171, p. 288, 1997.

97. Zugrav, M.: University of Alabama in Huntsville, private communication.

98. Reid, R.C.; Prausnitz, J.M.; and Poling, B.E.: *The Properties of Gases and Liquids*, 4th Ed., Pub.: McGraw-Hill Book Company, New York, NY, 1987.

99. Markham, B.L.; Greenwell, D.W.; and Rosenberger, F.: *J. Cryst. Growth*, vol. 51, p. 426, 1981.

100. Horner, C.J.; and Garito, A.F.: *Makromol. Chem.*, vol. 182, p. 19, 1981.

101. Garito, A.F.; Singer, K.D.; and Teng, C.C.: in *Nonlinear Optical Properties of Organic and Polymeric Materials*, Williams, D.J., Ed., ACS Symposium Series, vol. 233, American Chemical Society, Washington, DC, 1, 1983.

102. Etemad, S.; Baker, G.L.; and Soos, Z.G.: in *Molecular Nonlinear Optics*, J. Zyss, Ed.; Pub.: Academic Press, San Diego, CA, 1993.

103. Thakur, M.; and Krol, D.M.: *Appl. Phys. Lett.*, vol. 56(13), p. 1213, 1990.

104. Samoc, M.: The Australian National University, Laser Physics Centre, private communication.

105. Stegeman, G.I.; and Torruellas, W.: in *Electrical, Optical, and Magnetic Properties of Organic Solid State Materials*, A.F. Garito, A.K. Jen, C.Y-C. Lee, L. Dalton, Eds., MRS Symposium Proceedings, Materials Research Society, Pittsburg, PA, p. 397, 1994.

106. Walter, H.U., Ed.: *Fluid Sciences and Materials in Space ESA*, Pub.: Springer-Verlag, NY, 1987.

107. Antar, B.; and Nuotio-Antar, V.S.: *Fundamentals of Low-Gravity Fluid Dynamics and Heat Transfer*, Pub.: CRC Press, 1994.

108. Frazier, D.O.; Hung, R.J.; Paley, M.S.; and Long, Y.T.: *J. Crys. Growth*, to be published 1996.

109. Antar, B.N.: *Phys. Fluids*, vol. 30(2), p. 322, 1987.

110. Maxwell Garnett, J.C.: Philosophical Transactions of the Royal Society of London, vol. 203, p. 385, 1904; ibid., vol. 205, p. 237, 1906.

111. Ricard, D.; Rousignol, P.; and Flytzanis, C.: *Opt. Lett.*, vol. 10, p. 511, 1985.

112. Sipe, J.W.; and Boyd, R.W.: *Phys. Rev.*, vol. A 46, p. 1614, 1992.

113. Brust, M.; Walker, M.; Bethell, D.; Schiffrin, D.J.; and Whyman, R.: *J. Chem. Soc. Chem. Commun*., p. 801, 1994.

114. Paley, M.S.; Armstrong, S.; Witherow, W.K.; and Frazier, D.O.: *Chem. Mater.*, vol. 8(4), p. 912, 1996.

115. Bromberg, J.P.: Allyn and Bacon, *Physical Chemistry* Inc.: Boston, MA, p. 824, 1980.

116. Dorsinville, R.; Yang, L.; Alfano, R.R.; Zamboni, R.; Danieli, R.; Ruani, G.; and Taliani, C.: *Opt. Lett.*, vol. 14(23), p. 1321, 1989.

117. Logsdon, P.B.; Pfleger, J.; and Prasad, P.N.: *Synthetic Metals*, vol. 26, p. 369, 1988.

118. Erhardt, J.: *Galvanotechnik*, vol. 72(1), p. 13, 1981.

119. Naumann, R.J.: *Microgravity Science Technology*, vol. VIII/4, p. 204, 1995.

120. Riley, C.; Coble, H.D.; Loo, B.; Benson, B.; Abi-Akar, H.; and Maybee, G.: *Polymer Preprints*, vol. 28(2), p. 470, 1987.

121. Riley, C.; Coble, D.; and Maybee, G.: AIAA Paper 87–0510, 1987.

122. Riley, C.; Abi-Akar, H.; and Benson, B.: *J. Spacecraft and Rockets*, vol. 27(4), p. 386, 1990.

123. Dalton, L., et al.: *Advanced Materials*, vol. 7, p. 519, 1995; *Chemistry of Materials*, vol. 7, p. 1060 1995; *Appl. Phys. Lett.*, vol. 67, p. 1806, 1995.

124. Marder, S.R.; Perry, J.; Staehelin, M.; and Zysset, B.: *Science*, vol. 271, p. 335, 1996.

125. Aitchison, J.S.; Kean, A.H.; Ironside, C.N.; Villeneuve, A.; and Stegeman, G.I.: *Electron. Lett.*, vol. 27, p. 1709, 1991.

126. Villeneuve, A.; Yang, C.C.; Wigley, P.G.J.; Stegeman, G.I.; Aitchison, J.S.; and Ironside, C.N.: *Appl. Phys. Lett.*, vol. 61, p. 147, 1992.

129. Al-hemyari, A.; Aitchison, J.S.; Ironside, C.N.; Kennedy, G.T.; Grant, R.S.; and Sibbett, W.: *Electron. Lett.*, vol. 28, p. 1090, 1992.

128. Aitchison, J.S.; Villeneuve, A.; and Stegeman, G.I.: *Opt. Lett.*, vol. 18, p. 1153, 1993.

129. Yang, C.C.; Villeneuve, A.; Stegeman, G.I.; and Aitchison, J.S.: *Opt. Lett.*, vol. 17, p. 710, 1992.

130. Al-hemyari, A.; Villeneuve, A.; Kang, J.U.; Aitchison, J.S.; Ironside, C.N.; and Stegeman, G.I.: *Appl. Phys. Lett.*, vol. 63, p. 3562, 1993.

131. Lee, S.G.; McGinnis, B.P.; Jin, R.; Yumoto, J.; Khitrova, G.; Gibbs, H.M.; Binder, R.; Koch, S.W.; and Peyghambarian, N.: *Appl. Phys. Lett.*, vol. 64, p. 454, 1994.

132. Townsend, P.D.; Jackel, J.L.; Baker, G.L.; Shelburne, J.A.; and Etemad, S.: *Appl. Phys. Lett.*, vol. 55, p. 1829, 1989.

133. Rochford, K.B.; Zanoni, R.; Gong, Q.; and Stegeman, G.I.: *Appl. Phys. Lett.*, vol. 55, p. 1161, 1989.

134. Kim, D.Y.; Lawrence, B.L.; Torroellas, W.E.; Stegeman, G.I.; Baker, G.; and Meth, J.: *Appl. Phys. Lett.*, vol. 65, p. 1742, 1994.

REPORT DOCUMENTATION PAGE

Form Approved
OMB No. 0704-0188

Public reporting burden for this collection of information is estimated to average 1 hour per response, including the time for reviewing instructions, searching existing data sources, gathering and maintaining the data needed, and completing and reviewing the collection of information. Send comments regarding this burden estimate or any other aspect of this collection of information, including suggestions for reducing this burden, to Washington Headquarters Services, Directorate for Information Operation and Reports, 1215 Jefferson Davis Highway, Suite 1204, Arlington, VA 22202-4302, and to the Office of Management and Budget, Paperwork Reduction Project (0704-0188), Washington, DC 20503

1. AGENCY USE ONLY *(Leave Blank)*

2. REPORT DATE
March 1997

3. REPORT TYPE AND DATES COVERED
Technical Memorandum

4. TITLE AND SUBTITLE
Microgravity Processing and Photonic Applications of Organic and Polymeric Materials (MSFC Center Director's Discretionary Fund Final Report, Project No. 95–26)

5. FUNDING NUMBERS

6. AUTHORS
Donald O. Frazier,* Mark S. Paley,‡ Benjamin G. Penn,* Hossin A. Abdeldayem,‡ David D. Smith,* and William K. Witherow*

7. PERFORMING ORGANIZATION NAMES(S) AND ADDRESS(ES)
George C. Marshall Space Flight Center
Marshall Space Flight Center, Alabama 35812

8. PERFORMING ORGANIZATION REPORT NUMBER

9. SPONSORING/MONITORING AGENCY NAME(S) AND ADDRESS(ES)
National Aeronautics and Space Administration
Washington, DC 20546-0001

10. SPONSORING/MONITORING AGENCY REPORT NUMBER
NASA TM–108533

11. SUPPLEMENTARY NOTES
Prepared by Space Sciences Laboratory, Science and Engineering Directorate
*Marshall Space Flight Center ‡ Universities Space Research Association

12a. DISTRIBUTION/AVAILABILITY STATEMENT
Unclassified–Unlimited

12b. DISTRIBUTION CODE

13. ABSTRACT *(Maximum 200 words)*

Some of the primary purposes of this work are to study important technologies, particularly involving thin films, relevant to organic and polymeric materials for improving applicability to optical circuitry and devices and to assess the contribution of convection on film quality in unit and microgravity environments. Among the most important materials processing techniques of interest in this work are solution-based and by physical vapor transport, both having proven gravitational and acceleration dependence. In particular, polydiacetylenes (PDA's) and phthalocyanines (Pc's) are excellent nonlinear optical (NLO) materials with the promise of significantly improved NLO properties through order and film quality enhancements possible through microgravity processing.

Our approach is to focus research on integrated optical circuits and optoelectronic devices relevant to solution-based and vapor processes of interest in the Space Sciences Laboratory at the Marshall Space Flight Center (MSFC). Modification of organic materials is an important aspect of achieving more highly ordered structures in conjunction with microgravity processing. Parallel activities include characterization of materials for particular NLO properties and determination of appropriation device designs consistent with selected applications.

One result of this work is the determination, theoretically, that buoyancy-driven convection occurs at low pressures in an ideal gas in a thermalgradient from source to sink. Subsequent experiment supports the theory. We have also determined theoretically that buoyancy-driven convection occurs during photodeposition of PDA, an MSFC-patented process for fabricating complex circuits, which is also supported by experiment. Finally, the discovery of intrinsic optical bistability in metal-free Pc films enables the possibility of the development of logic gate technology on the basis of these materials.

14. SUBJECT TERMS
Nonlinear Optics, Organic- and Polymeric-Based Devices, Photonics, Electro-Optics, Microgravity Processing

15. NUMBER OF PAGES
60

16. PRICE CODE
NTIS

17. SECURITY CLASSIFICATION OF REPORT
Unclassified

18. SECURITY CLASSIFICATION OF THIS PAGE
Unclassified

19. SECURITY CLASSIFICATION OF ABSTRACT
Unclassified

20. LIMITATION OF ABSTRACT
Unlimited